

Portland State University

PDXScholar

Dissertations and Theses

Dissertations and Theses

1993

The Effects of Rapid Heating and Cooling on the Composition, Structure, and Superconducting Properties of Bi-Sr-Ca-Cu-O Compounds

Qing Duan

Portland State University

Follow this and additional works at: https://pdxscholar.library.pdx.edu/open_access_etds

Let us know how access to this document benefits you.

Recommended Citation

Duan, Qing, "The Effects of Rapid Heating and Cooling on the Composition, Structure, and Superconducting Properties of Bi-Sr-Ca-Cu-O Compounds" (1993). *Dissertations and Theses*. Paper 1322. <https://doi.org/10.15760/etd.1321>

This Dissertation is brought to you for free and open access. It has been accepted for inclusion in Dissertations and Theses by an authorized administrator of PDXScholar. Please contact us if we can make this document more accessible: pdxscholar@pdx.edu.

THE EFFECTS OF RAPID HEATING AND COOLING
ON THE COMPOSITION, STRUCTURE, AND SUPERCONDUCTING
PROPERTIES OF Bi-Sr-Ca-Cu-O COMPOUNDS

by
QING DUAN

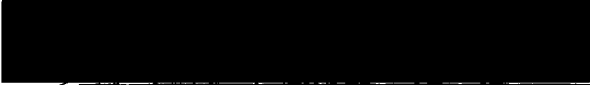
A dissertation submitted in partial fulfillment
of the requirements for the degree of

DOCTOR OF PHILOSOPHY
in
ENVIRONMENTAL SCIENCES AND RESOURCES:
PHYSICS

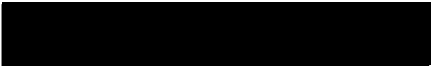
Portland State University
1993

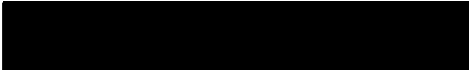
TO THE OFFICE OF GRADUATE STUDIES:

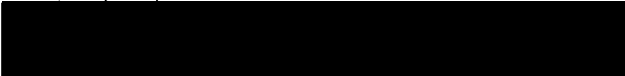
The members of the Committee approve the dissertation
of Qing Duan presented December 10, 1992.



John Dash, Chair


Makoto Takeo


Laird Brodie



David Paul



Bruce Brown


Richard Petersen


Carole Gatz

APPROVED:



John Rueter, Director, Environmental Sciences and
Resources Ph.D. Program


Roy Koch, Vice Provost for Graduate Studies and Research


AN ABSTRACT OF THE DISSERTATION OF Qing Duan for the Doctor of
Philosophy in Environmental Science and Resources: Physics
presented December 10, 1992.


Title: The Effects of Rapid Heating and Cooling on the
Composition, Structure, and Superconducting Properties
of Bi-Sr-Ca-Cu-O Compounds.

APPROVED BY THE MEMBERS OF THE DISSERTATION COMMITTEE:



John Dash, Chair



Makoto Takeo


Laird Brodie


David Paul


Bruce Brown


Richard Petersen


Carole Gatz

Bulk and thin film samples of $\text{Bi}_{2-x}\text{Pb}_x\text{Sr}_2\text{Ca}_2\text{Cu}_3\text{O}_y$ compounds

were prepared by suitable methods. The thin film and bulk samples were exposed to argon gas at temperatures of about 2000 °C and pressures of about 300 atm. in a ballistic compressor (BC) and then cooled at a rate of about 10^5 °C/sec. The samples before and after this treatment were examined and compared using a transmission electron microscope (TEM), a scanning electron microscope (SEM), an energy dispersive spectrometer (EDS), and an x-ray diffractometer (XRD). Resistance and magnetic susceptibility measurements were made to determine changes in superconducting temperature T_c .

Resistance and AC susceptibility measurements of bulk and thin film samples demonstrated that the T_c increased 3 - 6 K after the BC treatment, and step-shaped curves were often observed in the resistance versus temperature graphs.

The x-ray diffraction study revealed that the relative intensities of lines of the two high T_c phases clearly increased, and the relative intensities of lines of the low T_c phase decreased after the BC treatment.

Scanning electron micrographs of the exposed samples showed that surface melting had occurred, and the BC treatment affected the surface of samples to a depth of about 10 μm . Energy dispersive spectral analysis showed that oxygen loss occurred in the exposure process.

Transmission electron diffraction patterns showed that the crystal structure of the Bi-based compounds have an incommensurate modulation along the b-axis with different

periods of 25.4 Å, 38.7 Å and 72.6 Å. After the BC treatment, the lattice parameters of superconductors did not change, but the relative intensities of spots changed, the modulation of 72.6 Å disappeared, and the density of twist boundaries increased. These observations suggest that the treatment changed the density of structural defects and the atomic arrangement.

These studies tentatively indicate that the increase in structural defects was caused by oxygen loss. A very small oxygen loss increases the fraction of copper in Cu^{III} oxidation state, and thus increases the density of hole carriers in the Cu-O planes. This may be the reason why the T_c of Bi-based cuprate superconductors increased after the BC treatment.

ACKNOWLEDGEMENTS

There are many people who contributed both directly and indirectly in the completion of this dissertation.

I wish to express a great deal of appreciation and my sincere gratitude to Dr. John Dash for giving me unreserved guidance, solid support and advice throughout this project. He also gave me unstinted help during many difficult periods in my life.

I also appreciate very much the help of members of my committee: Dr. Brodie, Dr. Takeo, Dr. Brown, Dr. Paul, Dr. Petersen, and Dr. Gatz. They offered many useful suggestions.

Also, I wish to thank Dr. Takeo for introducing to me experimental methods of the ballistic compressor and for his helpful discussions. Appreciation is expressed to Dr. Brown for assistance with a computer program for x-ray diffraction.

I also owe a debt of gratitude to Dr. A. W. Sleight and Dr. Jinfan Huang of Oregon State University, who assisted me in the magnetic susceptibility measurements.

Thanks are extended to the remaining professors and staff in the Physics Department. Dr. Bodegom, Dr. Semura, and Dr Hsu, especially were very helpful during these years.

This work could not have been completed without the support of a number of people. The helpfulness with equipment

repair and modification of Rudolph Zupan, the late Garo Arakelyan, and Brian McLaughlin is appreciated. I also wish to thank my friends: Betsy Nicholas, Andreas Straub and Jeanne Hammond, and other graduate students in the Physics Department for their help and encouragement.

Finally, I deeply appreciate the help, understanding and support given to me by my husband, Xiqing Dai, my daughter Xiaobo, and my parents. Without their support, this study would have been impossible.

TABLE OF CONTENTS

	PAGE
ACKNOWLEDGEMENTS	iii
LIST OF TABLES	vii
LIST OF FIGURES	viii
CHAPTER	
I HISTORY OF SUPERCONDUCTIVITY.....	1
Introduction.....	1
Development of Experiments.....	2
Development of Theory.....	7
II THEORY OF HIGH TEMPERATURE SUPERCONDUCTIVITY..	14
Introduction.....	14
Structures of Oxide Superconductors.....	15
Common Features of Structure	
The System Bi-Sr-Ca-Cu-O	
Mechanism of Superconductivity	
Charge Transfer Model	
Structural Defects	
III EXPERIMENTAL METHODS.....	31
Introduction	31
Experimental Procedure.....	34
Preparation of Bi Compound Samples	
Experimental Procedures	
Operation of the Ballistic Compressor	
IV EXPERIMENTAL RESULTS AND DISCUSSION.....	45
Introduction.....	45

	vi
Experimental Results.....	46
Simple Meissner Effect Test	
Electrical Resistivity and Magnetic Susceptibility	
SEM Investigations	
EDS Investigation	
X-ray Diffraction Investigation	
TEM Investigation	
Discussion.....	84
Summary.....	98
V CONCLUSIONS.....	102
REFERENCES	104

LIST OF TABLES

TABLE		PAGE
I	Overview of Samples.....	37
II	A List of the Computed Peak Pressures and Temperatures for Samples Fired under Different Conditions in the Ballistic Compressor.....	43
III	List of Firing Conditions for Tested Samples.....	44
IV	Comparison of the Ratio of $\text{Cu}_{K\alpha}$ to Bi and the Ratio of $\text{O}_{K\alpha}$ to $\text{Cu}_{L\alpha}$ before and after BC Treatment.....	65
V	Lattice Parameters of Three Phases in Bi-Based System.....	66
VI	X-Ray Diffraction Data for Sample Thin#2 Before and After the Second Exposure in the Ballistic Compressor.....	72
VII	X-Ray Diffraction Data for Sample Thin#1 Before and After the Second Exposure in the Ballistic Compressor.....	74
VIIII	X-Ray Diffraction Data for Thin Film Sample Film#3 Before and After the Second Exposure in the Ballistic Compressor..	76

LIST OF FIGURES

FIGURE	PAGE
1. The ABO_3 Perovskite Structure.....	15
2. Schematic Representation of the Tentative Phase Relations in the Bi-Based System between $\text{Bi}_2(\text{Sr}, \text{Ca})\text{O}_4$ and $(\text{Sr}, \text{Ca})\text{CuO}_2$	18
3. Crystal Structure of the Compounds $\text{Bi}_2\text{Sr}_2\text{Ca}_{n-1}\text{Cu}_n\text{O}_{4+2n}$ with $n=1, 2,$ and 3.....	20
4. AC Susceptibility vs Temperature for Several Bulk Samples of Nominal Composition 4:3:3:4 of Bi Compounds Heat Treated under Different Conditions.....	33
5. Diagrams of the Ballistic Compressor at the P.S.U.....	41
6. The DC Resistance R as A Function of Temperature for the Bulk Sample #1 before Exposure to Hot, Dense Argon in the Ballistic Compressor, and after This Treatment.....	47

7.	DC Resistance vs Temperature for the Bulk Sample #2 before and after the First and Second Exposures in the Ballistic Compressor (12-22-89).....	48
8.	DC Resistance vs Temperature for the Bulk Sample #2 after the Second Exposure (7-27-90).....	49
9.	AC Resistance vs Temperature Curves of A Thin Pellet Thin#1 of Bi Compounds.....	50
10.	AC Electrical Resistance Versus Temperature Behavior for the Pellet Thin#2 before and after Exposure in the Ballistic Compressor.....	52
11.	AC Resistance Curves of A Thin Film Sample Film#2 of Bi-based Compounds.....	53
12.	The AC Susceptibility of the Thin Sample Thin#2 as A Function of Temperature before and after Second Exposure in the Ballistic Compressor.....	54
13.	The AC Susceptibility χ of the Thin Film Sample Film#1.....	55

14.	Magnetic Susceptibility vs Temperature of Thin Film Sample Film#3 before the First Exposure and after the Second Exposure in the Ballistic Compressor.....	56
15.	Magnetic Susceptibility of the Same Film Sample Film#3 after the Third Exposure in the Ballistic Compressor.....	56
16.	A Photograph and A Micrograph of the Unannealed Thin Film Sample (Unfilm) after the First Exposure in the Ballistic Compressor.....	58
17.	Scanning Electron Microscope Image of Thin Sample Thin#2.....	59
18.	SEM Cross-Section Micrograph of A Bulk Sample #2.....	61
19.	SEM Cross-Section Micrograph of the Pellet Thin#2.....	63
20.	EDS Data from near the Unexposed and Exposed Edges of the Sample Thin#2.....	64
21.	The Cu K α X-Ray Diffraction Pattern of Sample Thin#2.....	68
22.	In Low Angle Region, X-Ray Diffractographs for the Sample Thin#1.....	70

23.	Typical Electron Diffraction Pattern from the Bulk Sample #2 Along the [001] Direction.....	77
24.	Typical Electron Diffraction Pattern Along the [001] Direction.....	78
25.	Selected Area Electron Diffraction Patterns from A Thin Film Sample Film#3 in the [001] Zone Axes.....	80
26.	Electron Diffraction Pattern of A Twist Boundary ((001) plane) for Film Sample Film#1 Found after the First BC Treatment.....	82
27.	Electron Diffraction Pattern ((010) Plane) of A Twist Boundary Found in the Sample Film#1.....	83
28.	Schematic Diagram of the Proposed Superstructure of Bi-Based Compounds.....	96

CHAPTER I

HISTORY OF SUPERCONDUCTIVITY

INTRODUCTION

After the 1986 discovery of the cuprate high temperature superconductors (1), a large number of researchers were constantly searching for new materials with higher T_c , optimum treatment conditions to raise T_c of superconductors, and theoretical understanding of the new superconductors.

During the last three years more than 75 compounds with a T_c higher than 23 K have been discovered, and the experimental progress made in this period may surpass that in the previous years. The highest T_c is 125 K in the cuprate $Tl_2Ba_2Ca_2Cu_3O_{10}$ (2). The record highest critical magnetic field for cuprate superconductors is above 200 T (2), and the critical current density of $YBa_2Cu_3O_7$ at 77 K has reached 6×10^6 A/cm² for thin films and about 8×10^4 A/cm² for bulk samples (2). This progress on experiments may be due to improved sample quality and the availability of single crystals of various compounds.

Finding the material that becomes superconducting at a high temperature opens doors for more widespread use of superconductors. The high temperature superconductors have

been applied to microcircuitry and other frontiers of electronics, and some advanced superconductors will be used for power transmission and electric cars. High temperature superconductors may be suitable to conduct energy more efficiently. Therefore, further research work on high temperature superconductors may result in great benefits to the environment and conservation of energy resources.

This research work is focused on the effects of thermal treatment of Bi-based superconductors. Before describing this research, the main historical development of superconductivity is introduced.

DEVELOPMENT OF EXPERIMENTS

In the earlier history of superconductivity, two periods of the main activities of superconductors may be distinguished. The first one is the discovery of the resistanceless current and the existence of the critical current and the critical magnetic field. The second one is the discovery of the Meissner effect and the thermodynamic character of the superconductors. These are the cornerstones of the later development of superconductors.

In 1911, Heike Kamerlingh Onnes (3), a Dutch physicist, discovered the phenomenon of superconductivity in which the electrical resistance of mercury abruptly vanishes at a temperature of 4.2 K (called the critical temperature and denoted T_c). His further experiments (4) showed that the

current density which is a current per unit area passed through the superconductor was limited to a certain threshold value (denoted J_c). In 1914, he (5) also found there was a threshold value of the magnetic field (denoted H_c) when the resistance appeared in a specimen which was placed in the magnetic field. The second essential step in the development of superconductivity was the Meissner effect, discovered by Meissner and Ochsenfeld (6) in 1933. They found that an external magnetic field was expelled from the interior of a sample at T_c . This is due to the fact that the magnetic fields set up screening currents on surface of the sample, and the screening currents create an equal but opposite magnetic field, thereby repelling the external magnetic field. The difference between a perfect conductor and a superconductor is that the perfect conductor has no Meissner effect.

The zero resistance effect and Meissner effect are fundamental characteristic of superconductors, but not the only two. An abnormal thermal behavior of superconductors was found by W. H. Keesom and J. N. van den Ende (7) in 1932. The heat capacity of superconductors showed a jump at $T=T_c$ and an exponential decrease at lower temperature, which differs from those of a normal metal.

The discoveries of these properties of superconductors impelled the search for other superconducting materials. It was soon found that many metals, alloys and intermetallic compounds become superconducting when cooled to sufficiently

low temperatures. These low temperature superconductors could be classified into four groups:

- 1). Free-electron-like metals. The pure elements except the best conductors such as copper, gold, and silver become superconductors at very low temperature. The highest transition temperature is 9.26 K in niobium (8).
- 2). Strong-coupling materials. A Nb_3Sn alloy showed the highest T_c 18.1 K for many years (9).
- 3). Organic superconductors. The first organic superconductor was discovered by Jérôme et al. in 1980 (10), with T_c of 1 K in the $(\text{TMTSF})_2\text{X}$ series. At present, T_c is approaching 10 K in the other $(\text{BEDT-TTF})_2\text{X}$ series (11).
- 4). Heavy Fermion superconductors such as UPe_{13} , etc. $T_c < 1$ K is usual (12).

The first oxide superconductors, NbO and TiO , with T_c of 1 K were discovered in 1965 (13). These revealed a new class of materials to be explored. In the 75 years following the discovery of superconductivity, the transition temperature T_c had been gradually increased from the 4.2 K for Hg to 23 K for the compound Nb_3Ge (called low temperature superconductors, LTSC). This record held for 17 years. In 1986, the breakthrough to a considerably higher transition temperature was achieved by A. Bendorz and K. A. Müller (1). At that time superconductivity in the La-Ba-Cu-O system with T_c of 30 K was discovered. This discovery inspired scientists to seek new materials with better performance characteristics. In high

pressure experiments, C. W. Chu and M. K. Wu (14) found the critical temperature in La-Ba-Cu-O system shifted from 32 K to 40 K when measured under ten thousand atmospheres. They realized that the result could point a direction to seek a new chemical composition with smaller atoms that mimicked the high pressure effect. In 1987, C. W. Chu and M. K. Wu (15) announced that a ceramic oxide compound in the Y-Ba-Cu-O system becomes a superconductor at a temperature as high as 90 K (called high temperature superconductor, HTSC). In about 12 months, Bi-Sr-Ca-Cu-O compounds with transition temperatures up to 110 K, were discovered by Maeda *et al* (16). So far there are more than 75 high temperature superconductors with T_c higher than 23 K, which is the boiling point of liquid hydrogen. These are divided into three groups of cuprates (copper oxides), bismuthates (without copper), and fullerites ($(\text{Rb}, \text{Tl})_3\text{C}_{60}$). The maximum T_c is 125 K in the cuprate Tl-Ba-Ca-Cu-O system (17).

A large number of experiments demonstrated that the cuprate superconductors, which are the majority of the high T_c superconductors, have different properties than the low T_c superconductors, except zero electrical resistance and the Meissner effect. In the normal state, all the cuprate superconductors show unusual properties. They have a layered perovskite structure, and are very anisotropic (18). The Hall effect experiment showed that the carrier concentrations are much smaller than for the low temperature superconductors and

vary with doping (19). In the superconducting state, flux quantization experiments (20) have demonstrated similar features to the LTSC, in which the superconducting state is made up of paired carriers. Microwave and tunneling experiments (21), have shown that an energy gap is present in the superconducting state, but it is not clear if it follows the gap equation predicted by the BCS theory. J. Torrance (22) observed that T_c is a function of carrier concentration. When the carrier concentration n is greater than n_c (n_c denotes the optimum value which gives a maximum T_c), T_c drops. Change in n is achieved by changing the treatment conditions. At a sufficiently large value of n there is a superconducting to normal state transition. A number of other experiments illustrated differences in superconducting properties between HTSC and LTSC. For example, the superconducting coherence length (size of the Cooper pair, ξ_0) in the high temperature superconductors is extremely short, about 10^{-7} cm, but the ξ_0 in the conventional superconductors is about 10^{-4} cm. Because of the short coherence length, the cuprates possess a large penetration depth and are Type II superconductors (23). The heat capacity measurements (24) of high temperature superconductors showed a jump at T_c and a linear behavior with temperature, which is very different from the conventional superconductors. Jean et al (25) found that the positron lifetime (τ) undergoes a drastic change when temperature crosses T_c in HTSC but τ does not change with temperature in

LTSC. These experimental results suggest the existence of a charge transfer process in the high temperature superconductors. A large number of investigations showed many other interesting properties of high T_c superconductors, as well as those mentioned above. This enormous experimental progress in the years of development of superconductivity has greatly motivated the development of theory.

DEVELOPMENT OF THEORY

The discovery of the zero resistance effect and the Meissner effect aroused many scientists to seek scientific understanding and other features of the superconducting state. These efforts led to the creation of phenomenological theories. In 1934, Corter and Casimir (26) proposed the "two-fluid" model. This model assumed that below T_c the electrons in a superconductor divide into two parts: the "superconducting liquid" which passes through the sample without resistance and the "normal liquid" whose behavior is like the normal conduction electrons. With decreasing temperature, the "superconducting liquid" grows, while the "normal liquid" decreases and finally vanishes at $T=0$ K. The "two-liquid" model is based on the result of measurements of the specific heat of superconductors. It assumes that the entropy of the system is due to the particles in the normal state. At the transition temperature, there is only a change in the rate of entropy increase with temperature, which is

governed by the normal liquid, so superelectrons (assuming the conduction electrons are superconducting electrons) become normal conduction electrons. The two-fluid model is restricted in its applications because there is no real combination of two liquids in a superconductor. Its physical meaning is that the possible superconducting electrons in the superconductors would occur. After the discovery of the Meissner effect, F. London and H. London (27) presented equations to explain the macroscopic changes in magnetic properties caused by Meissner effect in a weak field. The London brothers described the electrodynamics of superconductors. Their equations are known as the London equations:

$$\nabla \times \mathbf{J}_s = -\frac{1}{\mu_o \lambda_L^2} \mathbf{B} \quad (1.1)$$

$$\frac{d}{dt} \mathbf{J}_s = \frac{1}{\mu_o \lambda_L^2} \mathbf{E}, \quad (1.2)$$

where \mathbf{J}_s is the supercurrent density on the surface of a superconductor, μ_o is the permeability of free space, λ_L the London penetration depth, which is a measurement of the depth of the flux density which dies away below the surface of a superconductor, \mathbf{B} is the applied magnetic flux density, and \mathbf{E} is the electric field strength. Equation (1.1) describes the

diamagnetic property of a superconductor. Equation (1.2) describes the resistanceless property. From the London equations, a current is induced in a superconductor when it is placed in an external magnetic field. The London theory gives a fairly good description of the properties of superconductors, but it can not explain the occurrence of superconductivity. The London theory is an approximation, and it is purely classical, so quantitative comparison of the experimental results of the penetration depth with the London prediction show a large differences. Various attempts to modify the London theory have been made. An important step in the phenomenological description of superconductors in strong fields was the Ginzburg-Landau theory (28), which is an alternative to the London theory. They introduced the insightful concept of a wave function to distinguish the normal state from the superconducting state. It is interesting to note that the Ginzburg-Landau theory uses quantum mechanics to predict the effect of a magnetic field.

In the Ginzburg-Landau theory, an order parameter is represented by the wavefunction, which defines the superelectron density. This is assumed to be

$$\Psi = |\Psi| \exp^{i\theta} \quad (1.3)$$

where Ψ is an effective wave function. The phase θ describes the macroscopic coherence properties of the superconducting

state, such that the quantity,

$$n_s = |\Psi|^2 \quad (1.4),$$

may be interpreted as the density of superconducting electrons, which vanishes for $T > T_c$. In terms of the wave function Ψ , Landau and Ginzburg expressed an expansion of Helmholtz free energy in a power series in terms of the order parameter. The difference in free energy of the superconducting state from that of the normal state can be expressed by the first two terms in this expansion. This theory predicts magnitudes of the critical magnetic field in terms of the expansion coefficients, and the behavior of superconductors in an external magnetic field. The validity of the Ginzburg-Landau theory was proven later on the basis of the microscopic theory. The only change made was that the number density of equation (1.4) is for Cooper pairs of charge $2e$ replaced the effective charge e^* appearing in this theory. The phenomenological theories mentioned above played an important role in the history of superconductors, but the main problem of explaining the nature of superconductivity remained unsolved. A discovery of the isotope effect which gave an important hint for the superconducting theory was made by Maxwell (29) and Reynolds (30) in 1950. The isotope effect described the relationship between the critical temperature and the isotopic mass as follows:

$$T_c M^{\frac{1}{2}} = \text{const.} \quad (1.5)$$

where M is the isotopic mass. The isotopic effect indicated that an electron-lattice interaction is involved in the superconductivity mechanism. After the discovery of the isotope effect, the current theory of superconductivity was soon developed. In 1956, L. N. Cooper (31) suggested that two electrons above the Fermi sea with an attractive interaction form a bound state. But he calculated the interaction for only a single pair of electrons which did not involve a very complicated many-body problem. A theoretical breakthrough, which explained the nature of superconductivity, was formulated by Bardeen, Cooper, and Schrieffer (the so-called BCS theory) (32) in 1957. The BCS theory predicted a microscopic mechanism in weak-coupling superconductors. At low temperature, an electron moving in the crystal disrupts the vibrational state of the lattice as it passes and excites the lattice. When the lattice returns to its ground state, it emits a phonon which is then immediately absorbed by another electron. This subsequently gives rise to a weak attraction that is in excess to the Coulomb repulsion force between the two electrons, although we never know which ones. In the quantum picture, these two electrons form a bound state (called Cooper pair) in which they possess the lowest energy, and have equal and opposite momentum. The wave function may

be written as

$$\Psi(r_1, r_2) = \nu \sum_{k_1, k_2} a_{k_1, k_2} \psi(k_1 \uparrow) \psi(-k_2 \downarrow) \quad (1.6)$$

where $\psi(k_1 \uparrow)$ describes an electron with wave number k_1 and spin up, and $\psi(k_2 \downarrow)$ term and electron with $-k_2$ and spin down. The ν is a normalization constant, and the $|a_{k_1, k_2}|^2$ gives the probability of finding the Cooper pair. If the temperature is raised, Cooper pairs are broken up by thermal agitation, and superconductivity disappears. The BCS theory explained the ground state, the excited state and the macroscopic properties of superconductors. The BCS theory described the temperature-dependent energy gap near the critical temperature by

$$\Delta(T)_{|T=T_c} = 1.74 \Delta(0) \sqrt{1 - \frac{T}{T_c}} \quad (1.7)$$

where $\Delta(T)$ is the energy gap, T is the temperature and $\Delta(0)$ is the energy gap at $T=0$ K. With increasing temperature the energy gap decreases and vanishes at $T=T_c$. This corresponds to a phase transition from the superconducting state to the normal state. The BCS theory also described a relationship between the zero temperature energy gap and the critical Temperature by the following fundamental expression:

$$\frac{\Delta(0)}{k_B T_c} = 1.764 \quad (1.8)$$

where k_B is Boltzmann's constant. This prediction agrees quite well with experimental (33) results which demonstrated the existence of the gap and its magnitude for many simple metallic superconductors. But experimental results in other materials such as organic superconductors (34) etc, produced deviations from the conventional BCS theory which was developed in the weak-coupling approximation. The reason for this is that the electron-phonon coupling in those materials is not weak. So the theory of strong coupling was proposed by Eliashberg (35) in 1960. Also, the discovery of high temperature oxide superconductors has opened a new chapter in superconducting history. The unusual properties such as short ξ and large energy gap, for the high T_c superconductors indicate that the conventional BCS theory has to be modified. So in the past five years many different theoretical concepts and models have been proposed and developed. The application of these to high T_c superconductors will be discussed in the next chapter.

CHAPTER II

THEORY OF HIGH TEMPERATURE SUPERCONDUCTIVITY

INTRODUCTION

The high T_c oxides have shown many unusual properties in both the normal and superconducting states. Traditional theoretical approaches (such as the BCS theory) to understanding these properties have failed to account for the strange behavior. For example, the isotope effect on T_c for the cuprate superconductors is extremely small because of very strong electron-phonon coupling. Thus, the fundamental physics requires further investigation. As indicated earlier, the high T_c superconductors have been divided into three groups: cuprates with the maximum T_c of 125 K, bismuthates with T_c about 30 K, and fullerites with T_c about 30 K. The main properties of the cuprate superconductors will be discussed because these constitute the majority of the high temperature oxide superconductors. And the unique properties of Bi-Sr-Cu-Ca-O compounds, which make them different from other cuprate superconductors, will be stressed.

STRUCTURES OF OXIDE SUPERCONDUCTORS

Common Features of Structure

The structures of high temperature cuprate compounds is very complex. But they commonly have the perovskite structure with a general formula ABO_3 . The basic structure of a perovskite compound is illustrated in Figure 1 in its idealized cubic form (36).

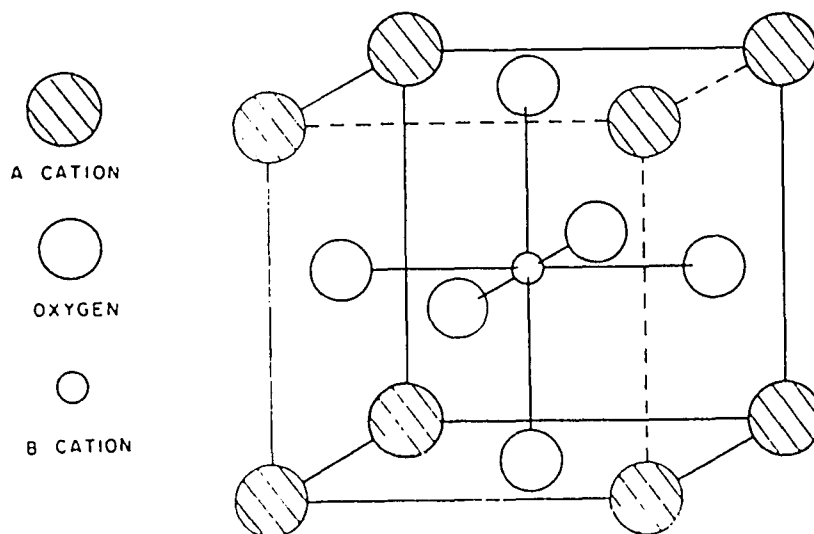


Figure 1. The ABO_3 perovskite structure.

The A and B in Figure 1 refer to different metallic atoms. The structure of cuprate superconductors consists of two or three such cells stacked one on the other.

A very important structural feature of all of the copper oxide superconductors is the presence of the two-dimensional CuO_2 square planes. The CuO_2 planes are separated by metal

atoms, for example, either an yttrium or a calcium atom. The copper atoms in the CuO_2 plane are located on the four corners and are strongly bounded to four oxygen atoms in the square planar form. The Cu-O distance in the cuprate superconductors is greater than the typical ionic bond length of Cu-O (37), so this indicates an enhanced contribution from covalent bonding. Because of this feature, the two-dimensional layers of Cu-O occur, and are perpendicular to the c-axis. These CuO_2 layers are separated by metal oxide layers such as BiO, TlO, SrO, or BaO, etc.

Another important feature of structure of the cuprate superconductors is that the Cu-O planes became conducting by doping. For example, the Cu-O layers in the parent La-Cu-O compounds do not have metallic characteristics, these compounds show semiconducting behavior (38). When Sr or Ba is added to the compounds, they show superconducting behavior. Electrons that are removed from the Cu-O planes to acceptors produced by the doping in the neighboring insulator layers increase, leaving more holes in the Cu-O layers for the hole-doped HTSC's. Or electrons are transferred to the CuO_2 planes from the surrounding layers for the electron-doped HTSC's. These compounds with doping show metallic behavior at room temperature, and become superconductors when cooled to low temperature.

High defect concentrations are also a common and important feature in high temperature cuprate superconductors.

The defects in the cuprate superconductors include oxygen vacancies, substitutional defects on the metal sites, atom displacements, etc. A. W. Sleight (39) suggested that the existence of the defects is thermodynamically stable due to the entropy contribution to the free energy of the phase at high temperature. However, it has been found that the existence of defects plays a very important role in oxide superconductors. The relationship of structural defects and superconductivity will be discussed in detail later.

The System Bi-Sr-Ca-Cu-O

The discovery of the high T_c Bi-Sr-Ca-Cu-O system has aroused great interest because of the absence of rare-earth elements in it and its T_c above 100 K. The structures and compositions of Bi compounds are very complex. The Bi-Sr-Ca-Cu-O system forms a series of compounds which can be described by the ideal formula $\text{Bi}_2\text{Sr}_2\text{Ca}_{n-1}\text{Cu}_n\text{O}_{4+2n}$ ($n=1,2,3,\dots$) (39). The Bi compound superconductors have three major phases, which are denoted by 2201 ($n=1$), 2212 ($n=2$), and 2223 ($n=3$) phase, respectively. It has been found that a broad range of composition exists for each phase of the Bi compounds (39). Figure 2 is a phase diagram of the Bi system provided by Ichinose (40). This shows tentative phase relations in this system between $\text{Bi}_2(\text{Sr,Ca})\text{O}_4$ and $(\text{Sr,Ca})\text{CuO}_2$. Three vertical lines in Figure 2 indicate the compositions of the phases 2201, 2212, and 2223, and so divide the phase diagram into

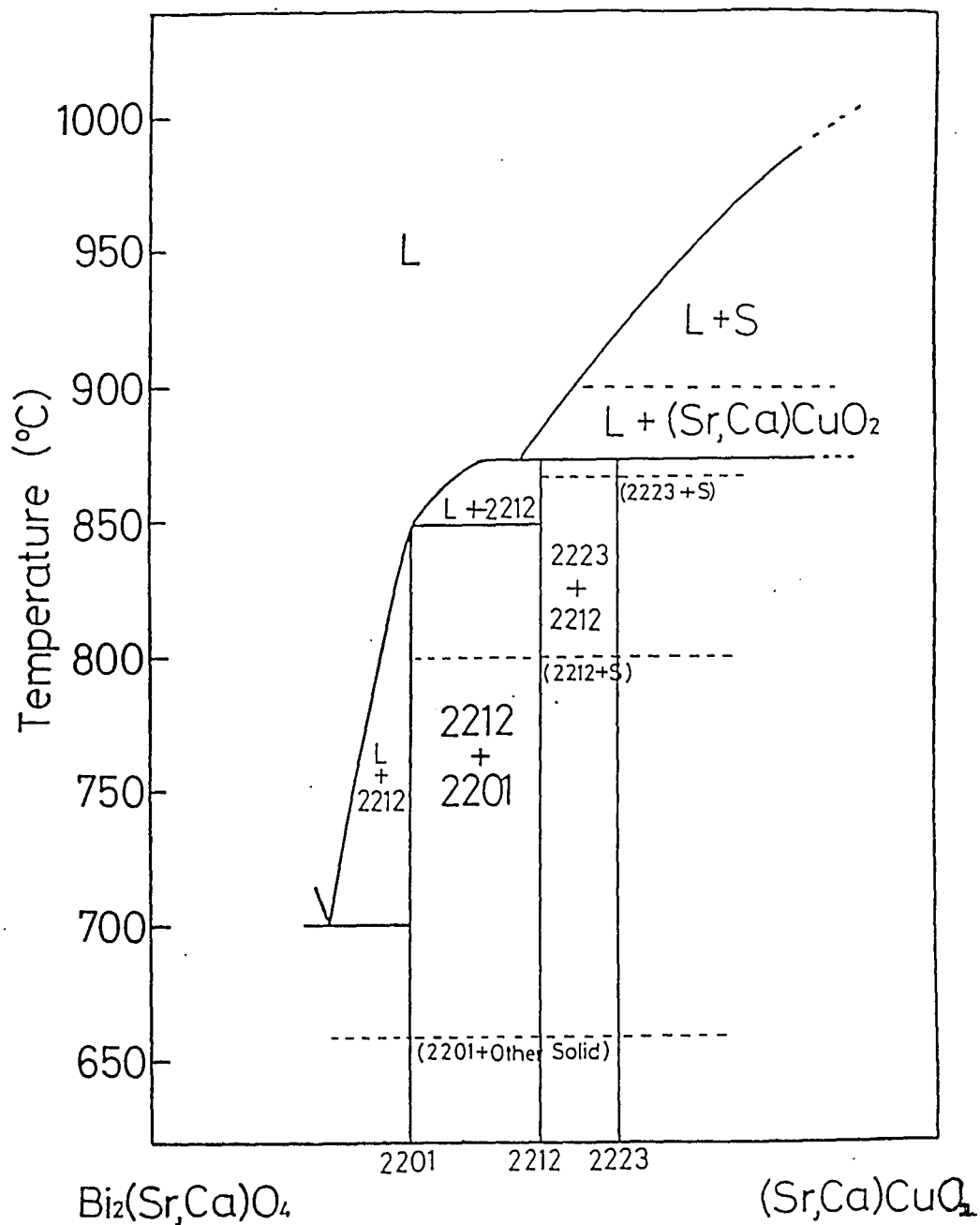


Figure 2. Schematic representation of the tentative phase relations in the Bi-based system between $\text{Bi}_2(\text{Sr,Ca})\text{O}_4$ and $(\text{Sr,Ca})\text{CuO}_2$.

different phase regions. The 2201 vertical line is close to the Bi-rich region, and the 2223 vertical line is close to the Cu-rich region. The phase diagram indicates that the 2201 phase and another unknown solid phase occur when the temperature is below 650 °C. As the heating temperature increases to above 650 °C and below 800 °C, a mixture of the 2201 phase, 2212 phase and another solid phase occurs, and the 2223 phase is absent. When the temperature exceeds 800 °C and around 880 °C that is a melting point for the Bi-based compounds, the 2223 phase appears and a mixture of 2212 and 2223 phases forms with the unknown solid phase. It can be thought that this is a phase intergrowth process.

The structure refinements of superconductors have been carried out using high resolution transmission electron microscopes, and x-ray and neutron diffractometers. Especially, neutron diffraction has played a major role in the study of superconductors because it can precisely determine the locations of oxygen atoms in a structure because of the difference of neutron scattering factors of light and heavy atoms (34). But the complete structures for these three phases of Bi compounds have not been determined because of their complicated structural defects. The basic and average perovskite structures of Bi compounds are shown in Figure 3 (42). A common characteristic of these Bi-based compounds is a crystal structure based on the stacking of BiO-BiO-SrO-CuO₂-Ca-sequences (43). The difference is that they contain one,

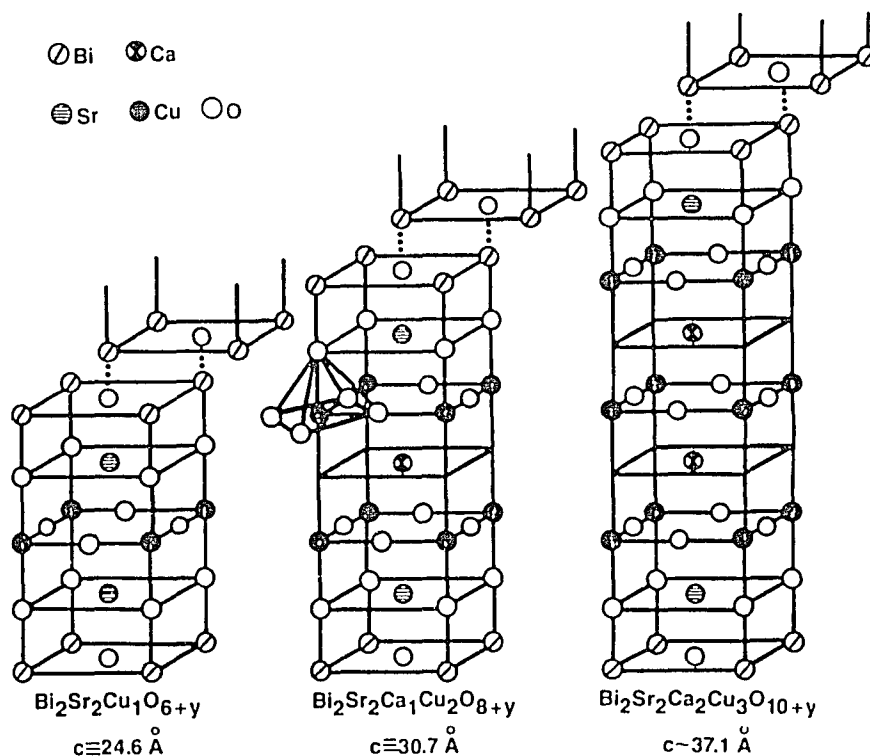


Figure 3. Crystal structure of the compounds $\text{Bi}_2\text{Sr}_2\text{Ca}_{n-1}\text{Cu}_n\text{O}_{4+2n}$ with $n=1, 2$, and 3 .

two, or three CuO_2 planes as n increases. T_c increases with an increasing number of CuO_2 planes but T_c peaks at $n=3$ and decreases for larger n . Single crystals of the 2201 and 2212 phases, which have T_c up to 10 K and 95 K, have been prepared (44). But the 2223 phase, which can have a T_c of about 110 K, is difficult to synthesize (39). The three distinct superconducting phases which exist in the Bi system have been indexed on a pseudotetragonal unit cell with parameters $a \approx b = 5.4 \text{ \AA}$ and $c = 24.4 \text{ \AA}$ ($n=1$), 30.7 \AA ($n=2$), 37.1 \AA ($n=3$) (43),

respectively. Transmission electron microscopy studies show that the c axis increases in length by 6 Å due to inclusion of an extra Cu and an extra Ca layer in Bi compounds (44). Based on this observation, samples showed signs of more than one superconducting transition by adding or moving the layers of Cu and Ca under different conditions. The intergrowth of these phases has been observed by high resolution electron microscopy (45).

Defects in the cuprate superconductors have been mentioned above, especially because these occur in high concentration and great complexity for the Bi compounds. High resolution electron microscopy images and electron diffraction patterns of Bi compounds showed modulation along the b-axis due to these defects (39).

Mechanism of Superconductivity

Since the discovery of high temperature superconductivity in Cu-based oxides, a great number of theoretical investigations have been undertaken in order to understand the mechanism of the occurrence of this new feature of superconductivity. The superconducting state in the cuprate materials is made up of paired carriers below T_c as has been demonstrated by microwave and tunneling experiments, but the pairing mechanism leading to T_c 's above 100 K still remains elusive. In the conventional BCS theory, superconductivity is generally explained by an electron-phonon

interaction in the pairing of electrons with weak coupling and the condensation of these pairs into a state of lower entropy. Because the parameter $\Delta(0)/E_F$ (E_F is the Fermi energy) in the cuprate superconductors is quite large, the BCS theory must be modified. Various types of theories have been proposed for the mechanism of superconductivity in recent years. Their range is from a conventional model (pairing mediated by various types of bosonic excitations) (46), to exotic models based on quasiparticles that obey anyonic statistics (46). And the bosonic excitations in the conventional models mainly include ordinary phonons, plasmons (47), and magnons (48), etc. Plasmons are similar to phonons, but phonons represent vibrational motion of the lattice, whereas plasmons correspond to collective vibrational motion of the carriers relative to the lattice. Plasmons have high frequency and strongly depend on the dimensionality of the system, which is so important in high T_c layered superconductors. Magnons are another attractive interaction between two electrons to form bound states, which exchange antiferromagnetic spin fluctuations. A simple explanation (49) is that the superconducting systems are generally not magnetically ordered. The free electrons in these materials repel local spin order, resulting in an attraction for free electrons with spins oriented to weaken the order.

Although many different explanations for the origin of superconductivity have been proposed, most of them have not

been confirmed in detail by experiments. At present, the electron-phonon interaction with strong coupling is accepted by many research groups because of its proven validity.

According to the results of experiments and analysis, the cuprate HTSC possess a short coherence length which is smaller than 100 Å (50) and a large energy gap, so the ratio $\Delta(0)/k_B T_C$ is about 2.5 (51), instead of the 1.76 in the traditional BCS theory. Both this ratio and also the short coherence length, are very important parameters because they indicate that only a fraction of the electronic states are involved in pairing.

Charge Transfer Model

The charge transfer model, which is one of many different models proposed in recent years, was proposed by J. D. Jorgensen (52). It is accepted by many researchers in this field because it is applicable to the oxide superconductors. As mentioned earlier, cuprate superconductors are obtained because either holes or electrons can be incorporated into the starting insulating composition in which Cu is divalent. Bi compounds are one of the hole-doped superconductors in which electrons are transferred from the CuO_2 layers to the surrounding layers. For copper oxide superconductors, it has been generally realized that the CuO_2 planes play an important role. By definition, Cu is in the divalent oxidation state (Cu^{II}) or trivalent (Cu^{III}) in the CuO_2 planes of p-type

superconductors, and the valence state of oxygen is two (O^{II}). Divalent copper Cu^{II} usually splits four short bonds to the O^{II} to form bond hybrids (53, 54), which are simply referred to as the conduction band. This conduction band is half filled, so it shows metallic properties and an antiferromagnetic behavior. At temperatures at and below T_c , holes (or electrons for n-type HTSC's) in CuO_2 planes should have favorable conditions to band together with strong coupling, thus forming the superconducting state (55). The holes concentration n_h in the CuO_2 planes for the Bi-based compounds is an important determining factor for the critical temperature and other properties of the HTSC. So in the copper oxide superconductors, superconductivity occurs in the CuO_2 planes, while the other layers such as BiO , SrO planes, etc, receive electrons transferred from CuO_2 layers and give rise to the coupling mechanism necessary for superconductivity. In the charge transfer model hypothesis, CuO_2 layers are the designated conduction layers, and their neighboring layers serve as charge reservoir layers. The charge reservoir layers have rather different effects on the charge transfer process. For example, strontium and calcium tend to be divalent, whereas bismuth can be univalent, trivalent or even in a higher valence state in the Bi compounds (56). Therefore, the BiO layers easily receive electrons and change oxidation state from the high valence state to the low one. The possible way for increasing the

number of holes in the CuO_2 planes is through bismuth ions. It is necessary to mention that the normal valence of copper for cuprate superconductors is not only Cu^{II} , but also Cu^{I} and a small fraction of Cu^{III} . The reason probably is due to the considerable range of composition of these compounds. A large number of experimental results have shown that T_c increases with decreasing Cu-O distance (53), or with increasing Cu^{III} concentration (55-57), or the intergrowth of the high T_c phases from the low T_c phase. But it is not in contradiction with the result that the concentration of carriers is a function of T_c in a certain range. A higher Cu^{III} concentration should decrease the average Cu-O distance because the $\text{Cu}^{\text{III}}\text{-O}^{\text{II}}$ distance is shorter than the $\text{Cu}^{\text{II}}\text{-O}^{\text{II}}$ distance, which is due to the removal of an electron from this Cu-O bond. And the higher Cu^{III} concentration results in a higher concentration of holes because of the removal of more electrons from the Cu-O planes.

The concentration of carriers in conduction layers is a key point in superconductivity. The number of carriers in the conduction layers is determined by the chemistry of the whole system and the number of electrons transferred between the conduction layers and the charge transfer layers. The number of charges transferred from the conduction layers to the charge reservoir layers is controlled by many factors such as structure, composition, etc. The typical carrier concentration in the CuO_2 planes for a Bi compound (2212

phase) is about 0.2 holes per Cu atom on each CuO_2 plane (58). The charge carrier concentration in the active CuO_2 layers is changed through chemical modification of the adjacent charge reservoirs layers. Such changes of the chemistry of the charge reservoirs layers are acquired by doping or the creation of structural defects.

Structural Defects

Most oxide superconductors are prepared by a variety of techniques such as solid-state reaction methods, *etc*, which result in rather broad ranges of composition which contain a number of complex defects in their structures. The defects in the cuprate superconductors include point defects, line defects, and plane defects such as twin boundaries. The point defects are the main type and include interstitial defects (interstitial oxygen atoms, for example), substitutional defects on the metal sites, atom displacements, and atomic vacancies, *etc*. Sleight (39) proposed that defects probably are thermodynamically stable due to the entropy contribution at high temperature, but may not be stable at low temperature. Therefore, part of these defects will be eliminated if the temperature is low enough. R. J. Cava (59) suggested similarly that the creation of defects at high temperature is due to the varying oxygen content and variable entropy that strongly influences the equilibrium state. The presence of defects after a rapid quenching to ambient temperature is due

to a frozen-in high temperature equilibrium state, in which the entropy introduced by the high temperature is employed. From the microscopic view, Jorgensen (52) provided a simple explanation for the formation of defects in the charge reservoir layers. The dimensions of the unit cell of cuprate superconductors are controlled by the actual dimensions of the CuO_2 conduction layers. And the atoms in the charge reservoir planes have to relax their position so that the dimensions of these planes can match those of the conduction plane. There is excess space in the charge reservoir layers. This creates interstitial defects or substitutional defects. For most cuprate superconductors, the dimensions of the conduction layers and the charge reservoir layers are not matched, but for the Bi-based compounds, the mismatch is so large that the structures display a clear incommensurate modulation. The defects in the charge transfer layers include metallic site vacancies, metal antisite defects (that is, the substitution of one type of metal atom onto the site normally occupied by another), oxygen vacancies and interstitial oxygen (60).

Jorgensen (52) proposed that the formation of defects in the charge reservoir planes can function to create carriers in the conduction layers and thus give rise to superconducting behavior. Because the structural defects of cuprate superconductors are so complicated, the process of how defects in the charge reservoir planes control the concentration of carriers in the CuO_2 planes has not been determined

completely. Although the mechanism of production of defects is different, some experimental results of doping support the last hypothesis. For example, if $\text{La}_2\text{CuO}_{2+\delta}$ is doped either with Sr on La sites ($\text{La}_{1.85}\text{Sr}_{0.15}\text{CuO}_4$) or with excess oxygen to form $\text{La}_2\text{CuO}_{4.08}$ (61), both compounds with the same doping level show the same T_c due to the same free electrons concentration. Jorgensen proposed also that defects occurring in the conduction layers may destroy superconductivity. A very important example of defects that destroy superconductivity occurs at the composition $\text{La}_{2-x}\text{Sr}_x\text{CaCu}_2\text{O}_6$ (62) with excess-oxygen defects in the CuO_2 planes. This material does not have a nonsuperconducting state, although the valence of copper in the CuO_2 planes is close to the optimum value. However, all agree that defects relate closely to the variation of oxygen content in the structure of superconducting samples because variation in the oxygen content will change the valence of copper. Nagoshi *et al.* (63) studied $\text{Bi}_2\text{Sr}_2\text{CaCu}_2\text{O}_y$ annealed in vacuum at various temperatures in order to evaluate in detail the effect of oxygen loss on the structure, hole concentration, and superconductivity. They found that T_c increases from 65 K to 92 K, which is accompanied by a small amount of oxygen loss (on the order of 10^{-3}). These interesting results support the charge transfer model, which suggest that charge redistribution in the structure is the origin of the large change of the carrier concentration in the CuO_2 planes.

It has been found that the T_c of the cuprate high temperature superconductors such as Y-based compounds (64-65) depends not only on the oxygen content but also on the specific ordering of the oxygen atoms in the Cu-O planes. Jorgensen (52) proposed that the ordering of defects will affect the properties of superconductors. An experiment was designed to monitor the effect of defect ordering on superconductivity (66). A single crystal of $\text{YBa}_2\text{Cu}_3\text{O}_x$ was heated to 500 °C in the appropriate oxygen partial pressure to keep the desired oxygen concentration in this sample, and then rapidly quenched to liquid nitrogen temperature to freeze the configuration of oxygen at high temperature. The T_c measurement was immediately performed. Then the sample was warmed to room temperature for a desired time. After this, T_c measurement was performed again. The same procedures for the same sample were repeated at different temperatures and for different times. Both T_c and structural measurements show that T_c systematically increased as defect ordering occurred. One explanation is that the oxygen atoms diffused to form an ordered configuration. This affected the carrier concentration in the CuO_2 planes. But it needs to be pointed out that the length scale of defect ordering is too short to be determined experimentally.

The charge transfer model works well to explain the major role of structural defects in the cuprate superconductors on superconductivity, so it has been accepted

by many research groups. But because of the complex structures of the oxide superconductors, there are still many questions which need to be answered. The progress in theory and experiments will continue.

CHAPTER III

EXPERIMENTAL METHODS

INTRODUCTION

The bismuth system contains three distinct superconducting phases, which have nominal compositions $\text{Bi}_2\text{Sr}_2\text{CuO}_6$ (2201), $\text{Bi}_2\text{Sr}_2\text{CaCu}_2\text{O}_8$ (2212), and $\text{Bi}_2\text{Sr}_2\text{Ca}_2\text{Cu}_3\text{O}_{10}$ (2223), respectively (38). The growth of single crystals of 2201 and 2212 phases has been accomplished (67). However, it is very difficult to prepare single crystals of the 2223 phase. In most cases a mixed phase structure forms and the highest T_c phase is always present in a low percentage in the Bi-based samples. The substitution of Pb in the Bi-Sr-Ca-Cu-O system greatly facilitates the formation and stabilization of the high T_c phase (68), but it does not affect the structural parameters. In this research work, bulk samples of Bi compounds with Pb-doping were the main subject of investigation. It has been observed that the superconducting properties of the high temperature oxide superconductors, such as critical temperature T_c , are extremely sensitive to the preparation processes, including annealing temperature, annealing time, pressure, and cooling rate, etc. Many researchers focused on the effects of thermal treatment of

cuprate superconductors. In recent years, much effort has gone to investigate the optimum treatment conditions to raise T_c of oxide superconductors and to improve the theoretical understanding of these phenomena. For example, the experimental results have shown that the high pressure coefficient dT_c/dp reaches 5.7 K/GPa (69) for Y-Ba-Cu-O compounds (1-2-4 phase and 1-2-3 phase), and is 2.0 K/GPa for the Bi system (2212 and 2223 phases) (70-73). C. W. Chu (74) has reported similar results. A long sintering time in such treatment processes is required for fabrication of the high- T_c superconducting phase and the elimination of the low- T_c phase (75, 76). G. C. Tu *et al.* (77) reported that the volume fraction of the high- T_c 2223 phase in the samples of Bi compounds increased from 0.43 to 0.51 while the samples were sintered at the same temperature for 51 hours and 76 hours, respectively. J. M. Tarascon *et al.* (42) have observed that T_c strongly depends on the heating temperature and the cooling rate. The T_c for samples of Bi compounds that were treated under different conditions, determined by ac susceptibility, are shown in Figure 4 (42). Comparison of (a) and (b) shows that T_c increased 10 K as the samples were heated at higher temperature with the same cooling rate. It is also noted in Figure 4 that T_c shows the highest value of 93 K for sample (c) which was heated at the highest temperature and cooled rapidly. The optimum synthesis temperature for the oxide superconductors is slightly below the melting point of the

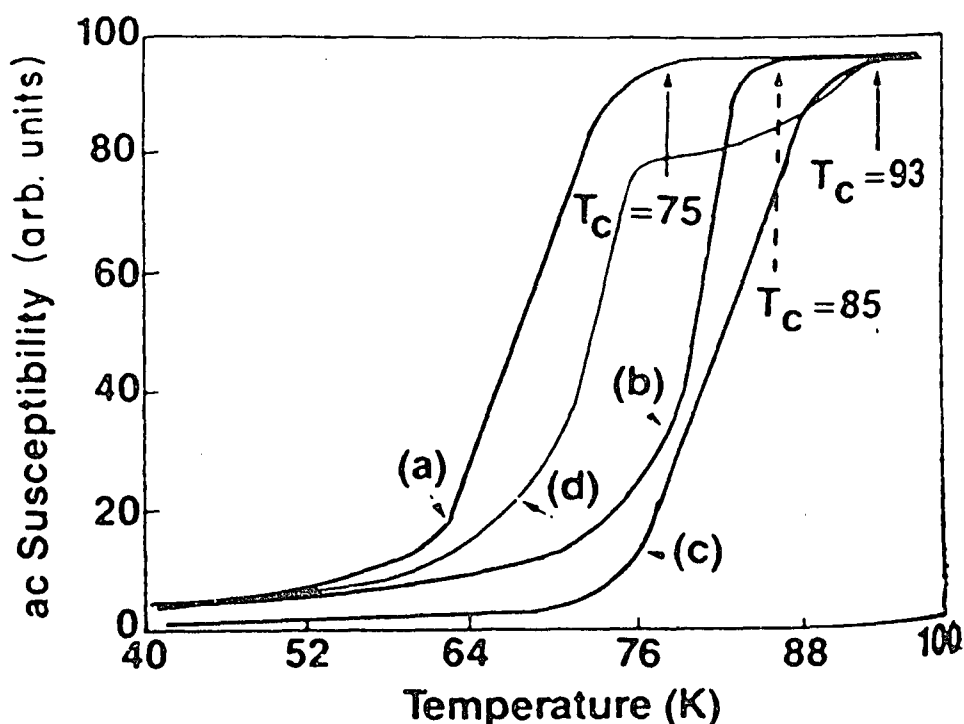


Figure 4. AC susceptibility vs temperature for several bulk samples of nominal composition 4:3:3:4 of Bi compounds heat treated under different conditions.

- (a) Sample heated to 840 °C and slowly cooled.
- (b) Sample heated to 860 °C and slowly cooled.
- (c) Sample melted at 1140 °C and cooled in two hours to 890 °C and maintained at this temperature for three days prior to being quenched.
- (d) Sample melted at 1140 °C and slowly cooled.

compounds, which is about 860 °C for Bi compounds (78). The most crucial step is the annealing. Samples are either directly annealed at high temperature in the appropriate environment of various gases such as oxygen with different cooling rates, or are directly quenched in liquid nitrogen (79). The range of cooling rate is usually from 1 °C/sec to

100 °C/sec. Yoshimura et al. (80) have reported on preparation of amorphous films by rapid quenching after rapid melting, with a cooling rate of 10^5 K/sec. They concentrated on the melt-quenching technique of preparing completely amorphous films, but did not investigate the effect of slower cooling rates. These amorphous samples must be further heat treated at high temperature (1073 K, then quenched) to become superconductors. In this thesis, the relationship between heat treatment and the properties of superconductors, and the mechanisms involved have been further investigated. This research is focused on the effects of rapid heating and cooling on the composition, structure and superconducting properties of the bismuth-based cuprate superconductors. A unique apparatus, a ballistic compressor (BC) in the physics department of Portland State University, can produce dense gas at about 6000 K for a millisecond, which is followed immediately by a cooling rate of about 10^5 °C/sec. This apparatus has been utilized to produce repeated rapid thermal cycles after which changes in the superconducting properties and structure were observed.

EXPERIMENTAL PROCEDURE

Preparation of Bi Compound Samples

The superconducting ceramic samples of nominal composition $\text{Bi}_{2-x}\text{Pb}_x\text{Sr}_2\text{Ca}_2\text{Cu}_3\text{O}_y$ with $x=0.2$ were prepared by the conventional solid state reaction in air. The synthesis is as

follows: the high-purity oxides or carbonates of the constituent metals, i.e. Bi_2O_3 (99% pure, Em Industries, Inc), Pb_3O_4 (99.5% pure, J. T. Baker Chem. Co.), SrCO_3 (98.5% pure, General Chem. Div.), CaCO_3 (99.95% pure after 2 hours at 285 °C, Mallinckrodt. Inc.), and CuO (99.5% pure, J. T. Baker Chem. Co.) were employed as the starting materials. The CaCO_3 was dried in advance by heating in air at 200 °C for about 2 hours to obtain a dry compound. These powders were weighed approximately in the ratio $[\text{Bi}]:[\text{Pb}]:[\text{Sr}]:[\text{Ca}]:[\text{Cu}] = 2.1:0.23:1.5:1.0:1.2$ to give the stoichiometry 2:2:2:3. The powders were thoroughly mixed and ground by hand in a mortar and pestle. Then, the mixed powder was calcined at 800 ± 7 °C for 16 hours in air. The sinter was removed from the furnace and reground in the same way as before to ensure sample uniformity. Using a hydraulic press (Buehler 20-1311), the powder was pressed into pellets of 0.5 inch in diameter, with various thickness from 0.8 mm to 2.5 mm at a pressure as high as 10,000 p.s.i. and a temperature of about 100 °C. The pellets were placed together on edge in a mullite tube and then heated in air at a temperature of $865 \text{ °C} \pm 7 \text{ °C}$ for 60 hours. Then the pellets were removed from the furnace and directly dropped into liquid nitrogen. The cooling rate is estimated to be less than 100 K/sec. Some quenched bulk samples were glued to a thin slice of glass with super glue to facilitate grinding to thinner samples. These samples were ground on the SiC abrasive papers with 400 mesh abrasive (400

openings per inch) and then 600 mesh. After grinding, samples on the glass substrates with thickness of about 0.8 mm-1.0 mm are called thin samples. Here the research on only two bulk samples with thickness of about 2.5 - 3.0 mm and two thin samples of the same batch of specimens will be described. These are denoted #1 and #2 for the bulk samples without and with Pb doping, respectively, and thin#1 and thin#2 for the thin samples.

Research was also performed on one annealed thin film sample of the Bi-based compound on a LaAlO_3 substrate (denoted film#1), which was obtained in Jan. 1991. Another annealed and one unannealed thin film samples of this compound on SrTiO_3 substrates (denoted film#2 and unfilm, respectively), were received in Sept. 1991. These three samples were from Superconducting Components, Inc., and were made by sputtering. The dimensions for these samples were $1.0 \times 1.0 \text{ cm}^2$ and the thickness of films was about 2000 Å. There were gold bands on the surface of sample film#2 for electrical contacts, so it was divided into three portions. Another thin film sample of Bi-Sr-Ca-Cu-O compound on a MgO substrate (denoted film#3), which was received from the laboratory of A. W. Sleight at Oregon State University, was also used in this research work. It was reported that this thin film sample was deposited on a MgO substrate by spin coating from liquid solution precursors (81). One piece $2.0 \text{ mm} \times 10.0 \text{ mm}$ that was cut from each film sample was not exposed in the ballistic

compressor so that its properties could be compared with the same sample after BC treatments. Table I gives an overview for these samples, which were investigated in this research work.

TABLE I
OVERVIEW OF SAMPLES

Bulk Samples	thick sample	#1	~ 2.8 mm	with Pb
		#2	~ 2.5 mm	without Pb
	thin sample	thin#1	~ 0.8 mm	with Pb
		thin#2		
Thin Film Samples		film#1	on LaAlO ₃	without Pb
		film#2	on SrTiO ₃	
		unfilm	on SrTiO ₃	
		film#3	on MgO	

For the transmission electron microscopy study, superconducting particles were scraped carefully from both the unexposed and exposed surfaces of samples by using a single edge razor blade. Then the particles were put between two glass slides and further milled to produce smaller particles. The smallest particles were deposited onto a grid coated with a thin evaporated gold film, which was held vertically with a forceps and carefully tapped to remove all particles which did not adhere by electrostatic attraction. By this method of specimen preparation, the structure of the superconductor particles can be precisely determined by electron diffraction,

using the superimposed electron diffraction pattern of the gold substrate film for calibration.

Experimental Procedure

After sample preparation, a qualitative test of the Meissner effect was made by observing whether or not a small magnet was repelled above the surface of pellets immersed in liquid nitrogen, so the presence of superconductivity could be determined.

Superconducting properties were analyzed by measurement of the temperature dependence of electrical resistance of the bulk and thin samples carried out by a standard four-point probe configuration (82) using a constant current. Electrical contacts of these samples were made by thin silver foils attached to the surface of the samples with a conducting, air-drying, silver paste (colloidal silver liquid). The samples were placed on a styrofoam cup and immersed in liquid nitrogen. Two leads from a stable current source are used to inject a low current into each sample in turn. Two voltage probes are mounted on the sample between the current leads to give a measurement of sample resistance. The temperature of the bulk samples was monitored with a copper-constantan thermocouple inserted in a hole drilled into the side of the pellet. The T_c measurements were also determined with the same thermocouple attached on the surface of the thin samples. The range of measuring currents used in direct current T_c

measurements was about 30 mA - 100 mA. For some thin samples and thin film samples, a.c. resistance measurements were made in the similar four terminal method in the range 77.7-150 K by using an AC susceptometer (Lake Shore model 7000), which is in the laboratory of A. W. Sleight at Oregon State University, with a known AC constant of 400 A/m, frequency 100 Hz, and current 100 μ A. The temperature was increased 1 K per min in the range 77.7-95 K, and 3 K per min in the range 100-150 K.

AC magnetic susceptibility measurements were also performed using the same susceptometer consisting of a primary coil and a pair of secondaries connected in series opposition (83). Samples move between upper and lower secondaries in order to eliminate noise that is introduced by the instrument and the detection system. The sample is subjected to a small AC magnetic field, and the flux variation due to the sample is picked up by a sensing coil surrounding the sample and the resulting voltage induced in the coil is detected. The measured induced voltage in the presence of a sample is proportional to the susceptibility. In this study, Meissner diamagnetism measurements (χ) of both thin (0.8 mm) and film samples were made in the range 4.2 K - 150 K. The same AC susceptometer was used with similar conditions except that the temperature was increased 3 K / min in the range 4.2-77.7 K and frequency was either 80 Hz or 100 Hz, depending on the size of samples.

Phase identification of all samples was carried out at

room temperature with an X-ray diffractometer using monochromatized Cu-K α radiation with $\lambda=1.54050 \text{ \AA}$. A PHILIPS XRG-3000 x-ray diffractometer (XRD) was used to record diffraction spectra of samples with a scanning speed of 1.0 $^{\circ}$ /minute and a chart speed of 0.5 inch per degree in the range $2^{\circ} < 2\theta < 60^{\circ}$.

The microstructural characterization was performed using scanning electron microscopy (SEM). An ISI SS40 SEM was used. The chemical composition analysis of the samples was performed with a LINK energy dispersive spectrometer (EDS) attached to the SEM. A detector window with thickness of about $0.1 \mu\text{m}$ was used. The energy of the beam for Bi-based superconductors was 20 kev. A LINK Analytical AN-10000 software package was used for spectrum analysis.

Transmission electron microscopy was performed with a HITACHI HU-125 transmission electron microscope (TEM) equipped with a $\pm 10^{\circ}$ universal tilt specimen holder.

The measurements mentioned above were made on the same samples before and after exposure in the ballistic compressor in order to investigate the BC treatment effects on superconductivity, morphology, composition, and structure.

Operation of the Ballistic Compressor

The ballistic compressor is an unique apparatus at Portland State University which can be used to produce rapid heating and cooling cycles. A detailed report of its

structure and characteristics has been described elsewhere (84). A structural cross section diagram of the ballistic compressor is shown in Figure 5 (85).

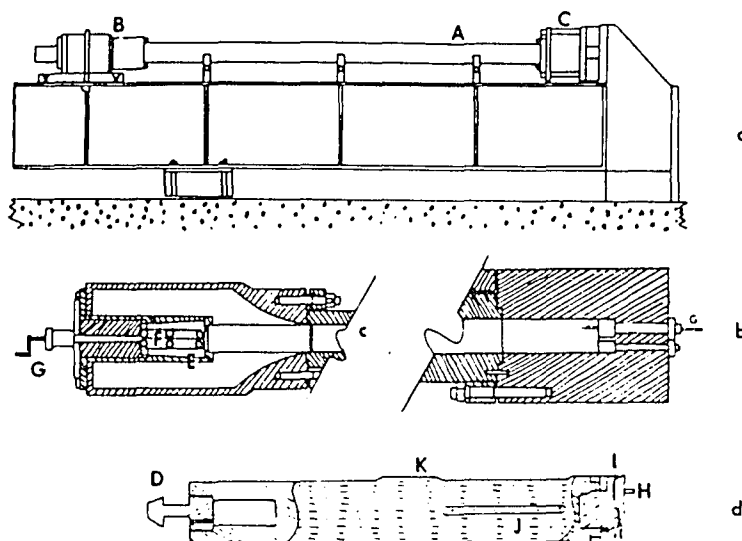


Figure 5. Diagrams of the ballistic compressor at the P.S.U. (a) A side view of the ballistic compressor. (b) A pressure transducer is mounted in the end wall of the high pressure head. (c) The piston holding and release mechanism are contained in the driving gas reservoir. (d) Diagram of the piston (52.6 cm long).

In Figure 5-a, (A) is a horizontal 2.90 m long tube, (B) and (C) are the driving gas reservoir and the high pressure head, respectively. Bulk samples were mounted on the piston head with an annular metal holder, which was screwed onto the surface of the piston head. Thin pellets and film samples were mounted on the piston head with double sticky tape. In the prefiring position, the rear of the piston was held inside

the driving gas reservoir and isolated from the driving gas pressure by an O-ring. The ballistic compressor was filled with argon gas, which is inert to the chemical elements of the sample.

Before firing, the driving gas reservoir was filled with argon up to either 20.4 atm. or 23.8 atm., and the long tube was filled to 0.5 atm. or 1.0 atm. When released, the piston moved forward. The maximum possible distance that the piston moved in the ballistic compressor is 2.77 m. The gas in the high pressure head was compressed in half a millisecond, and the temperature was as high as 6000 K and the pressure was about 3000 atm. Then the piston rebounded, so samples were exposed to hot, dense gas for a short time, followed by a cooling rate as fast as about 10^5 °C/sec.

In the BC treatment process, the peak pressure was detected by a PCB piezotronics pressure transducer (Model 105A), which is mounted at the end of the side wall of the high pressure head. The electrical signals then were displayed on an oscilloscope (Tektronix RM35A) and recorded by a polaroid camera. In order to characterize the thermodynamic conditions of the test gas in the ballistic compressor, gas leakage, viscous friction, and heat losses were taken into account in the theoretical analysis of the piston's motion. Also, a simulated test experiment was made to determine the peak pressure and the minimum volume of the test gas. In the simulated test experiment, a copper rod about 5.0 inches long

was inserted and glued in a hole at the center of the piston head. After firing, it was bent into a different length that showed the minimum volume of the test gas after firing in the ballistic compressor at different conditions. Then a few trials with different values of the piston gap and different temperature gradients at the wall were run on the computer until the computed peak pressure and minimum volume of the test gas agreed with experiments. After these steps, the peak pressures and temperatures in the BC treatment processes were determined uniquely. The computed peak pressures and temperatures of samples fired under different conditions in the ballistic compressor are listed in Table II.

TABLE II

A LIST OF THE COMPUTED PEAK PRESSURES AND TEMPERATURES
FOR SAMPLES FIRED UNDER DIFFERENT CONDITIONS
IN THE BALLISTIC COMPRESSOR

P_{test} atm.	T_{test} K	P_{res} atm.	T_{res} K	D_{min} cm	Peak P atm.	Peak T K
0.5	297.9	20.4	297.9	2.90	644.4	2938.8
1.0	297.7	20.4	297.7	7.50	233.0	1504.2
1.0	297.6	23.8	297.6	6.60	335.9	1833.7

The samples of thin#1, thin#2, and film#3 were fired at 1833 K and 335 atm., samples film#1, film#2, and unfilm were treated at 1504 K and 233 atm., and bulk samples #1 and #2 were fired at 2938 K and 644 atm. The thermal conditions were limited to avoid fracture and melting of samples in the

ballistic compressor. Samples usually were treated one, two or three times to maximize the effects of the BC treatments. Different firing conditions for these samples are listed in Table III. After BC treatment, samples were removed from the ballistic compressor and examined under TEM, EDS, SEM, and X-ray. T_c was also measured.

TABLE III
LIST OF FIRING CONDITIONS FOR TESTED
SAMPLES

		Name of Sample	Firing Times in BC	Peak P atm.	Peak T K
Bulk Samples	Thick Sample	#1	one time	644	2938
		#2	two times	644	2938
	Thin Sample	thin#1	one time	335	1833
		thin#2	two times	335	1833
Thin Film Samples		film#1	one time	233	1504
		film#2	three times	233	1504
		unfilm	three times	233	1504
		film#3	three times	335	1833

CHAPTER IV

EXPERIMENTAL RESULTS AND DISCUSSION

INTRODUCTION

In this thesis Bi-Sr-Ca-Cu-O samples treated in the ballistic compressor were studied in order to elucidate the details of effects of rapid heating and cooling on the structure, composition, and superconducting properties of superconductors. X-ray diffraction was used to determine the crystalline phases in the samples, while transmission electron microscopy and scanning electron microscopy with energy dispersive spectrometry were the main techniques used to characterize the microstructure and composition of the samples. In addition, microstructural observations were correlated with DC and AC resistance and AC magnetic susceptibility measurements. T_c data were determined in the "warming up" process as the temperature at which the electrical resistance dropped almost to zero. A small remaining resistance at temperatures lower than T_c was due to the contact resistance through which a small current passed, due to the finite input impedance of the voltmeter. The onset of superconductivity was taken as the temperature at which the tangent of the resistance against temperature curve for the

normal state intersected the tangent of the part where the resistance dropped precipitously. The purpose of this research was to find the changes in T_c and microstructure of superconductors caused by the BC treatment. So the measurements of resistance versus temperature for bulk and thin samples before and after exposure in the ballistic compressor were performed in the same directions which were located relative to the locations of thermocouple and with nearly the exact same experimental conditions, such as currents, heating rate, etc. From these results, the relationship between defects and superconductivity in this Bi-based system will be discussed in terms of the charge transfer model.

EXPERIMENTAL RESULTS

Simple Meissner Effect Test

A small magnet was placed above either unexposed or exposed bulk samples (0.5 to 3 mm thick) which were cooled in liquid nitrogen. The magnet was repelled to various degrees by the cooled sample, depending on the strength of the Meissner effect. The procedure of this experiment has already been described elsewhere (86). Sometimes it was difficult to decide the difference between unexposed and exposed samples, so this is only a qualitative test to help in determining the qualities of superconductor samples.

Electrical Resistivity and Magnetic Susceptibility

The effect of ballistic compressor exposure on the superconducting transition temperature for the bulk sample #1 of a Pb-free, Bi-based compounds is shown in Figure 6 (87). This shows that T_c increased from 100 K before this treatment to 106 K afterward. The measurement current was 30 ma. Duplicate measurements on the same sample in both conditions gave agreement within 1 K. The R-T curve that was obtained from the same sample after BC treatment, shows a two-step superconducting transition. The higher temperature steps are at 116 K and 137 K. Similar resistance measurements were made on bulk sample #2, which is a Bi-system superconductor doped

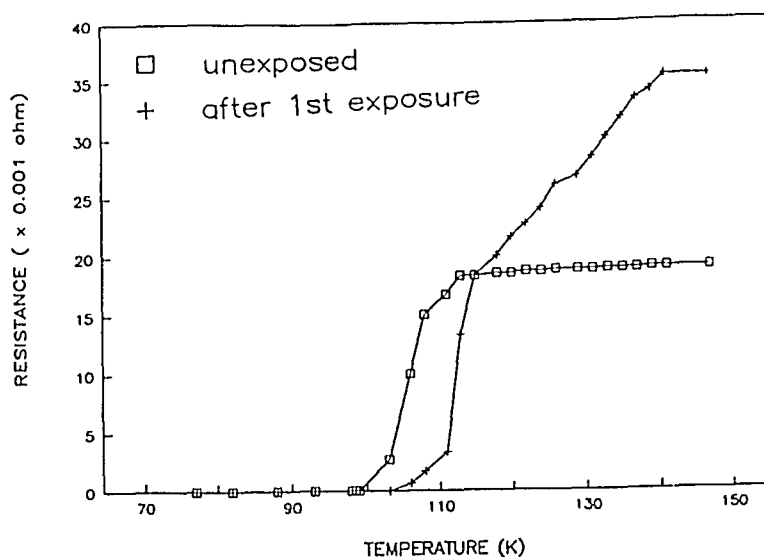


Figure 6. The DC resistance R as a function of temperature for the bulk sample #1 before exposure to hot, dense argon in the ballistic compressor, and after this treatment.

with Pb (Figure 7) (88). A constant current of 100 ma was used because the T_c of sample #2 showed the highest value under this condition. The electrical resistance versus temperature curves for the unexposed pellet and after the first exposure indicate transitions with T_c 's at 85 and 89 K, respectively. Although the second exposure of sample #2 in the ballistic compressor (measured in Dec, 1989) produced no further enhancement of critical temperature T_c , it did reduce the transition width, which is the temperature range from the onset temperature to T_c . This was reduced from 18 K to 12 K.

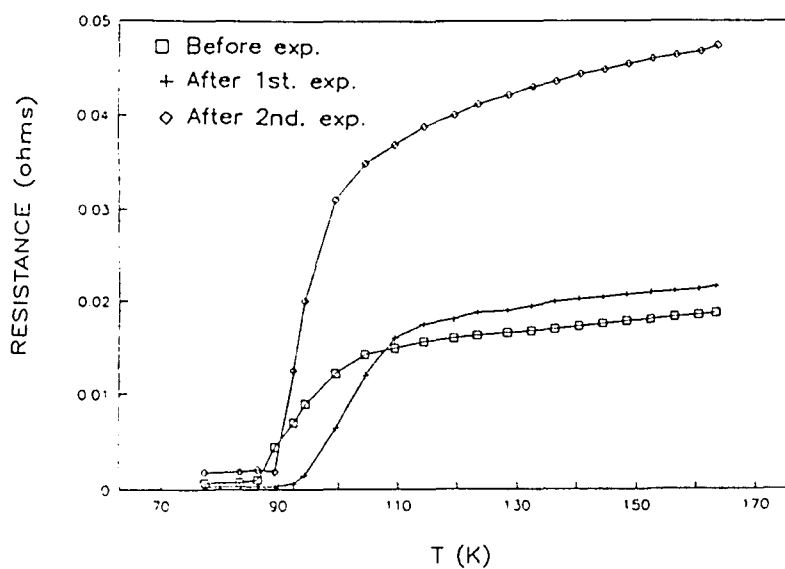


Figure 7. DC Resistance vs temperature for the Bi-Pb-Sr-Ca-Cu-O sample #2 before and after the first and second exposures in the ballistic compressor (12-22-89).

In order to determine the reproducibility of the resistance measurement, the same sample that was exposed in the ballistic

compressor two times, was remeasured after seven months (July 27, 1990) under almost the same conditions (Figure 8). Comparison of T_c for sample #2 in Figure 7 and Figure 8 shows that the second measurement (7-27-90) is in conformity with the first measurement (12-22-89) of the sample after the second BC exposure. The higher resistance shown in the 7-27-90 results was probably due to the slightly different placement of electrical contacts, which were remade due to deterioration of the silver paint.

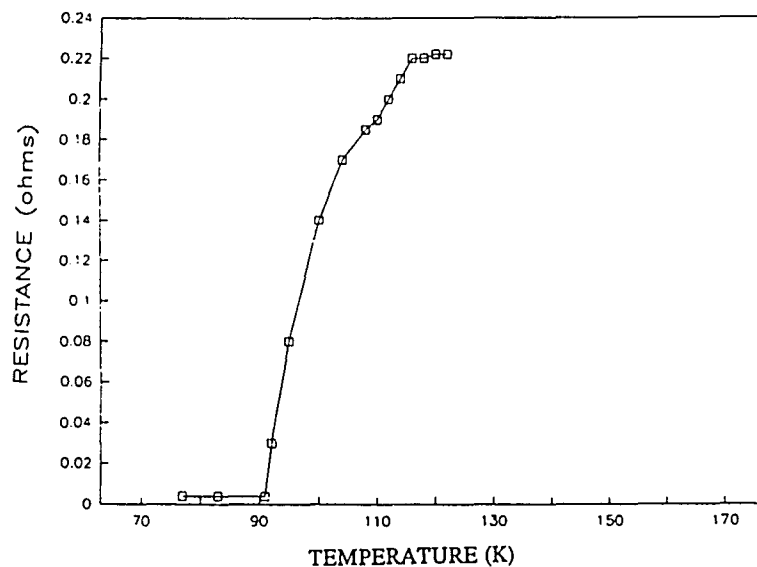


Figure 8. DC resistance vs temperature for the bulk sample #2 after the second exposure (7-27-90).

Similar observations apply to superconductivity for the other bulk samples. About 80% of the samples that were tested showed similar results after the BC treatment, whether or not these samples contained Pb. About 20% of these samples either

broke during exposure in BC or showed no change in T_C .

The temperature dependence of AC electrical resistance of the thin samples (about 0.6mm thick) thin#1 and thin#2 were measured also, and the results are shown in Figure 9 and Figure 10, respectively. A comparison of the AC resistance

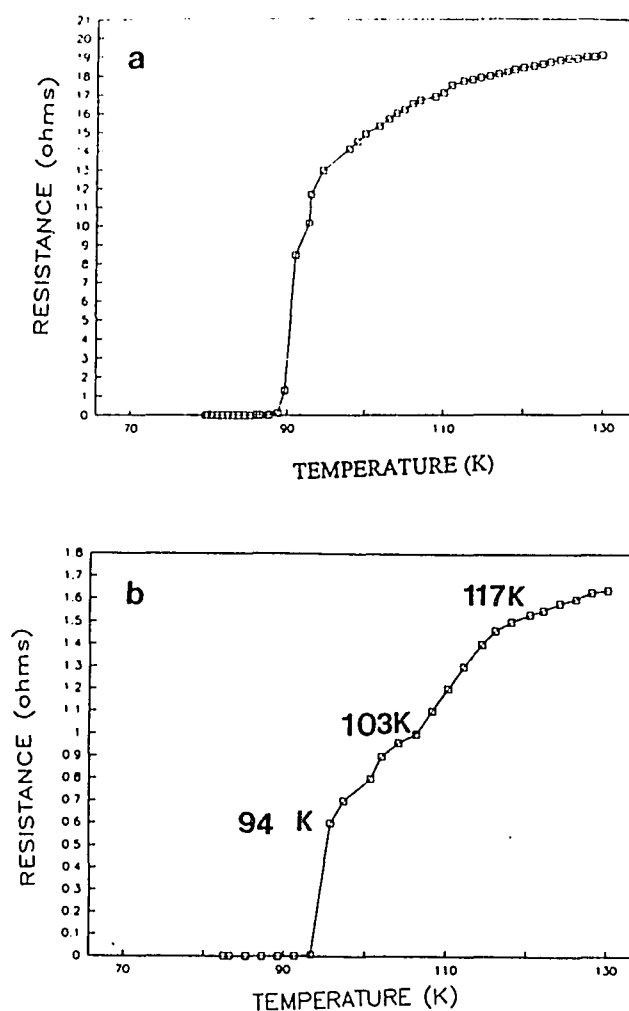


Figure 9. AC resistance vs temperature curves of a thin pellet thin#1 of Bi compounds. (a) before and (b) after the BC treatment.

versus temperature curves in Figures 9 (a) and (b) shows the zero resistance temperature changed from 87 K to 92 K after exposure in the ballistic compressor. It should be noted that the R-T curve after BC exposure shows a different shape with a step-like behavior, which is similar to the result obtained for the bulk samples #1 after the BC treatment. From Figure 9-b, it appears that the steps at 117 K, 103 K and 94 K, can be deduced. Figure 10 (a) shows that the T_c of the sample thin#2 increased about 2 K. This was measured on 3-4-92. The critical temperature results for the same sample obtained after more than one month is shown in Figure 10 (b).

An interesting result for the thin film sample film#2 is that the resistance/temperature curve shows semiconducting behavior before the BC treatment (Figure 11 (a)). After the third exposure in the ballistic compressor, the electrical resistance curve in Figure 11 (b) displayed the same semiconducting behavior. From this experiment, it indicated this treatment did not change the semiconductor properties of the thin film sample.

The diamagnetic susceptibility was observed for the thin and film samples, thin#2, film#1, and film#3. The susceptibility versus temperature curves for the thin sample thin#2 before and after the second exposure are presented in Figure 12 (a), which was measured on 4-20-92. The transition to superconductivity (onset of the Meissner signal) is uniformly situated at about 113 K, in agreement with the

resistance measurements. The slope of the susceptibility-temperature curve changed greatly at about 95 K. The Meissner signals are not smooth but contain one or more steps in the region between about 113 K and 97 K. Thus, these susceptibility/temperature curves show different slopes before and after exposure in the BC, and also display an increase of the slope after the second exposure.

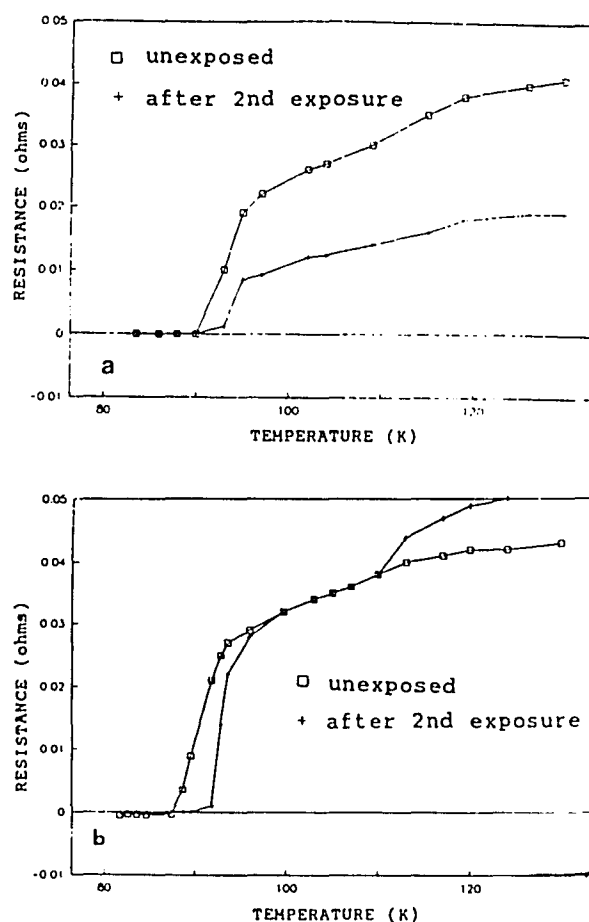


Figure 10. AC electrical resistance versus temperature behavior for the pellet thin#2 before and after exposure in the ballistic compressor. (a) first trial on 3-4-92; (b) second trial on 4-25-92.

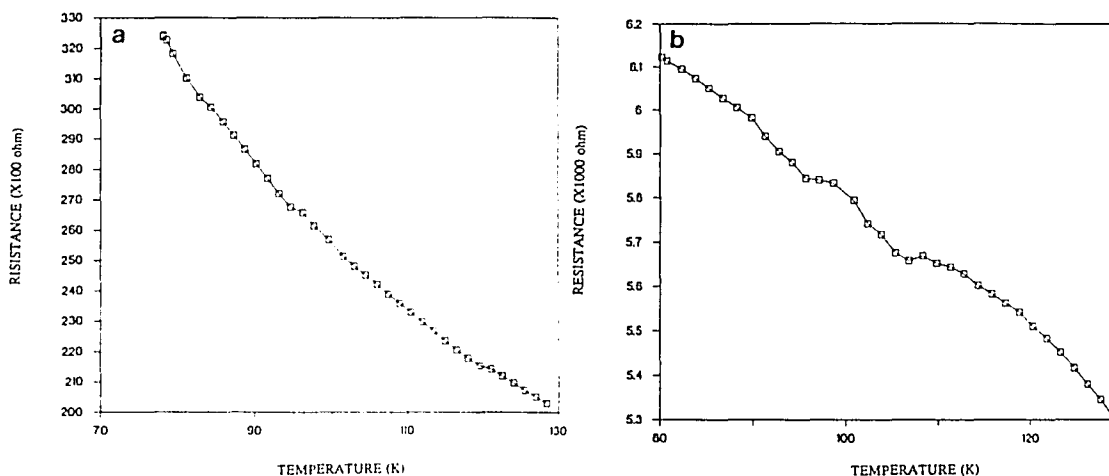


Figure 11. AC resistance curves of a thin film sample film#2 of Bi-based compounds. (a) before and (b) after the BC treatment; both display semiconducting behavior.

In Figure 12 (b), the exposed sample thin#2 was tested for susceptibility again on 9-19-92. It shows good reproducibility with the results obtained on 4-20-92.

The critical temperatures determined by AC susceptibility for thin film samples film#1 and film#3 are shown in Figure 13 and Figure 14. From Figure 13, note that the magnetic susceptibility versus temperature curves for film#1 before and after the BC treatment are not smooth, but are accompanied by electrical noise. This is probably due to the small volume of the thin film, because the susceptibility χ of a sample depends on the experimental parameters as given by the following relationship:

$$\chi = \alpha v / (VfH) \quad (4.1)$$

where α is the calibration coefficient, v is measured voltage,

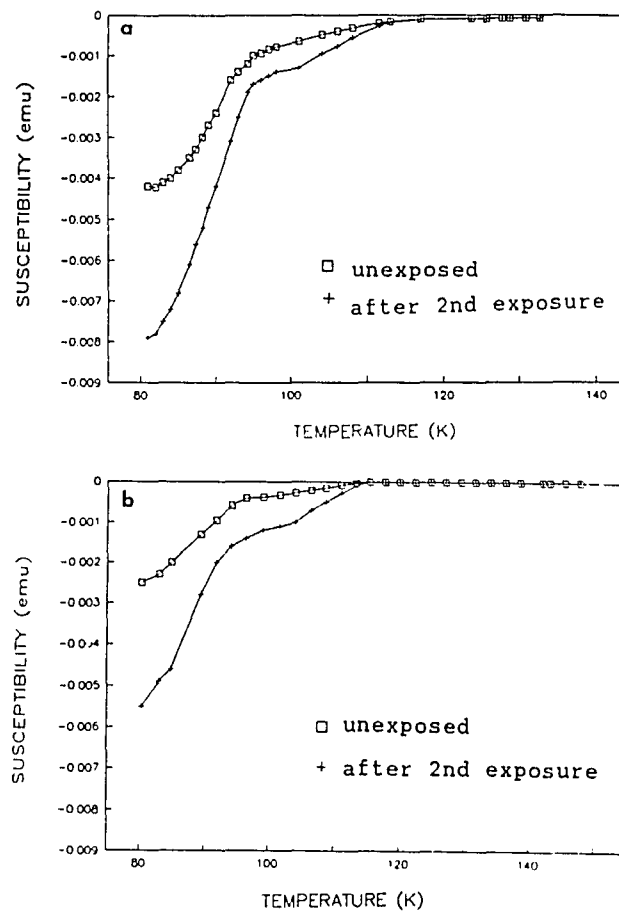


Figure 12. The AC susceptibility of the thin sample thin#2 as a function of temperature before and after second exposure in the ballistic compressor. (a) first trial on 4-20-92. (b) second trial on 9-19-92.

V is the sample volume, f is the frequency of the AC field, and H is the magnetic field. However, Figure 13 shows that the superconducting behavior was improved and T_c was 91 K after the BC treatment.

A similar change in T_c of sample film#3 was observed after the second ballistic compressor exposure (Figure 14)

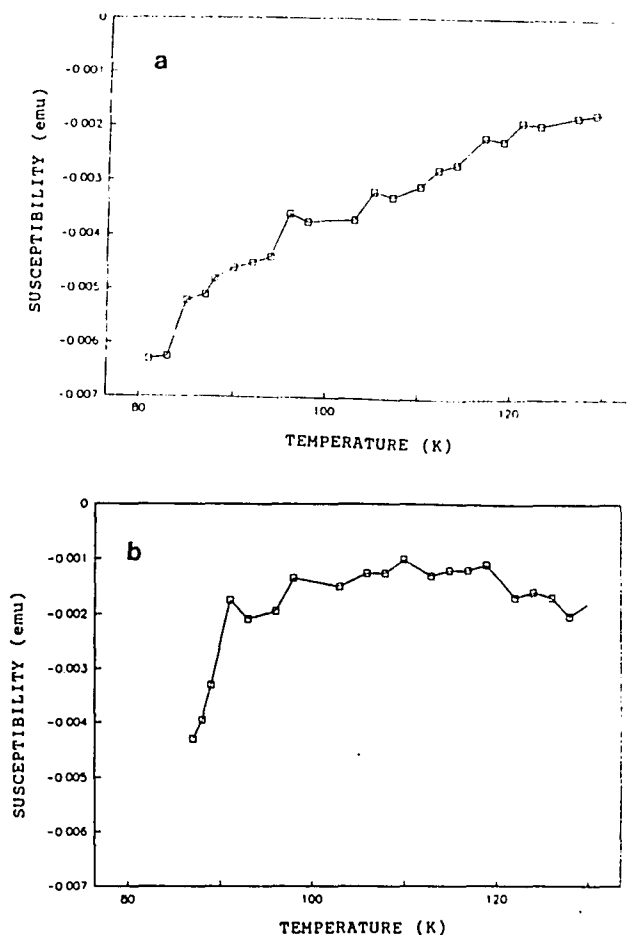


Figure 13. The AC susceptibility χ of the thin film sample film#1. (a) before and (b) after first exposure in the ballistic compressor.

(88). The results of the BC treatment show that T_c increased about 3 K, with step-like behavior in the χ -T curve. It is worth noting that the superconducting behavior of the sample film#3 after the third exposure (Figure 15) shows a T_c of 120 K. This may be one of the highest T_c for a thin film sample of the Bi compounds because it is extremely difficult to grow a thin film of a Bi-based compound with T_c above 100 K.

Unfortunately, this result could not be reproduced because there were no more thin film samples available.

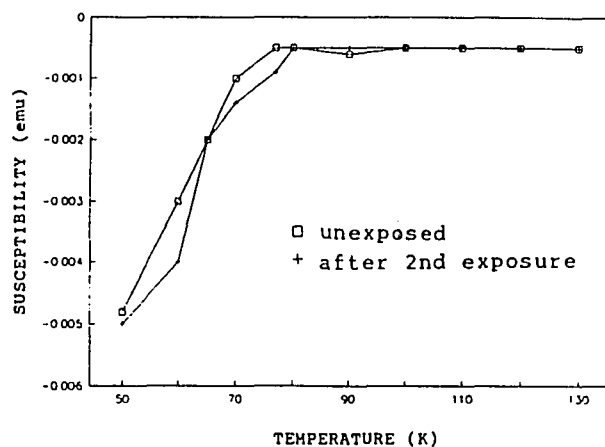


Figure 14. Magnetic susceptibility vs temperature of thin film sample film#3 before the first exposure and after the second exposure in the ballistic compressor.

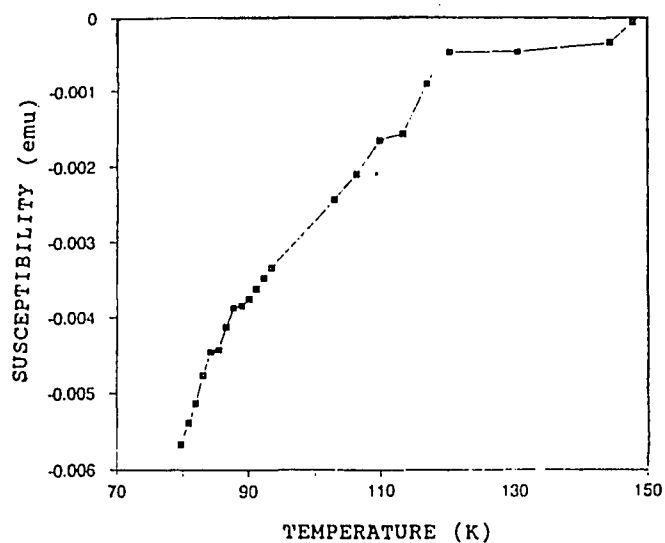


Figure 15. Magnetic susceptibility of the same film sample film#3 after the third exposure in the ballistic compressor.

SEM Investigations

The unannealed thin film sample (unfilm) did not undergo heat treatment after it was deposited on a SrTiO_3 substrate. This film easily came off the substrate when treated in the BC. A photograph of the whole area of a film sample after BC exposure, is shown in Figure 16 (a). This shows that the film, which was uniform before BC treatment, is very nonuniform after the treatment. From the difference in color of the sample surface, it is apparent that the sample is not uniform after exposure in the ballistic compressor. The SEM image, which is an enlargement of the brown colored area on the surface of this film sample, displays a bubble-like surface (Figure 16 (b)).

The ballistic compressor treatment changed the black color of the exposed surface of superconductors slightly to a copper color, and also increased porosity. Figure 17 shows scanning electron micrographs (1600X) of the sample thin#1 without (a) and with (b) BC treatment, which were from the different location so that to show the obviously the BC treatment effect. In Figure 17 (a), the sample had a granular structure and there were plate-like grains before exposure. These plate-like crystals generally grow in random directions and form a porous structure. It has been found that the needle-like grains are the low T_c phase (2201), and the plate-like structures are the high T_c phases (89-91). After the BC treatment, part of this surface was changed, but some plate-

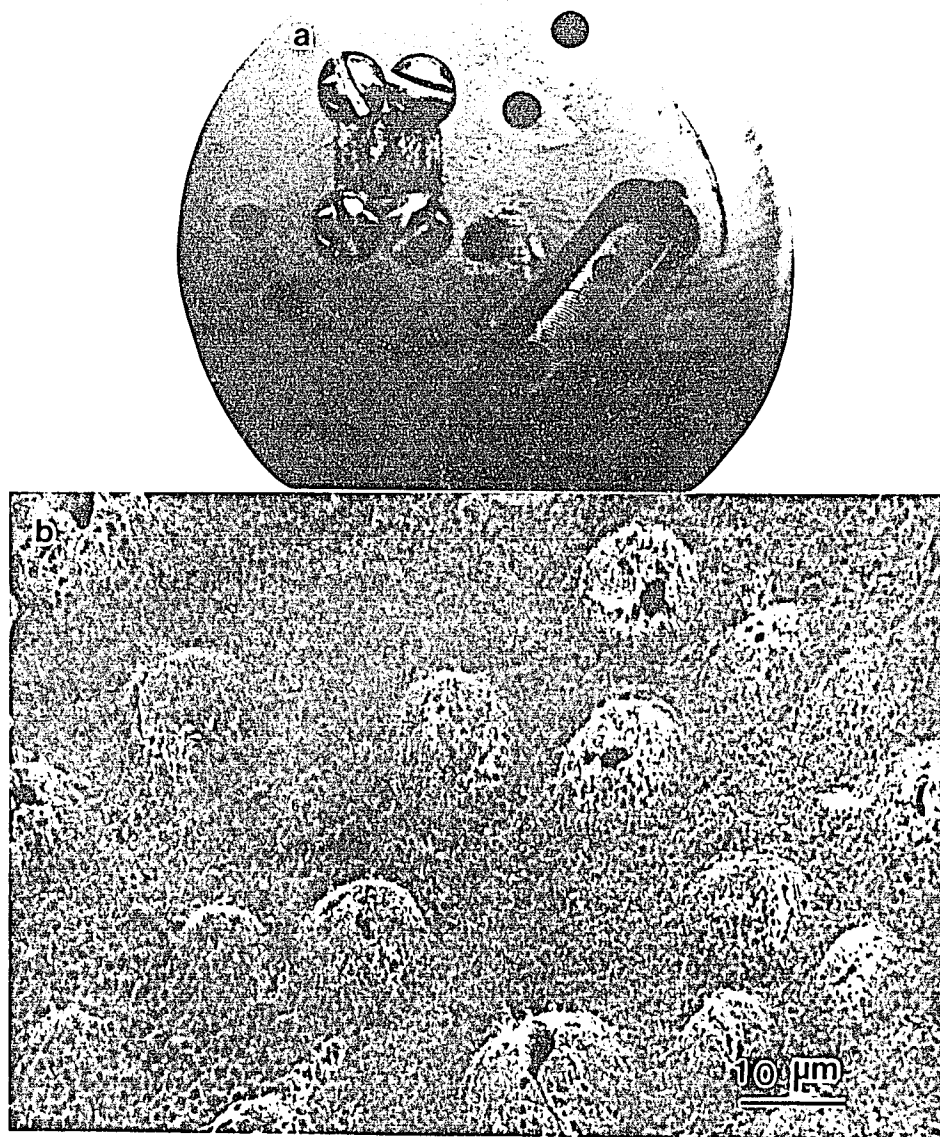


Figure 16. A photograph and a micrograph of the unannealed thin film sample (unfilm) after the first exposure in the ballistic compressor. (a) a photograph of whole area of the exposed sample. (b) a SEM image of brown colored area on the surface.



Figure 17. Scanning electron microscope image of thin sample thin#2. (a) before and (b) after exposure in the ballistic compressor. The left arrow in (a) indicates plate-like particles which are thought to be the high T_c phases. The right arrow in (a) indicates a needle-like particle which may be the low T_c phase.

After the BC treatment, part of this surface was changed, but some plate-like crystals still remained.

In order to determine the depth of the heat-affected zone in the sample after ballistic compressor treatment, bulk sample #2 was ground on edge using 600-mesh sandpaper. This ground cross section was observed with the SEM. The SEM image of the cross-section is shown in Figure 18. When samples were fired in the ballistic compressor, the hot, dense gas only affected the surface of samples to a depth of about $10\text{ }\mu\text{m}$ which displayed a smoother and more dense condition. At high magnification (3450X), the SEM cross-section micrograph in Figure 18 displays clearly the distinction between unaffected and affected layers. The BC treatment only affected the surface of the sample to a depth of about 10^{-3} cm . Therefore, the BC treatment is called a "skin effect".

EDS Investigation

It is commonly found that the chemical composition of cuprate samples varies considerably from grain to grain of one sample. An average elemental composition analysis of a sample usually was performed with the electron beam scanning an area of about $1.2\text{ mm} \times 1.2\text{ mm}$ on the sample's surface at low magnification. In order to compare the compositions of samples before and after exposure in the ballistic compressor,

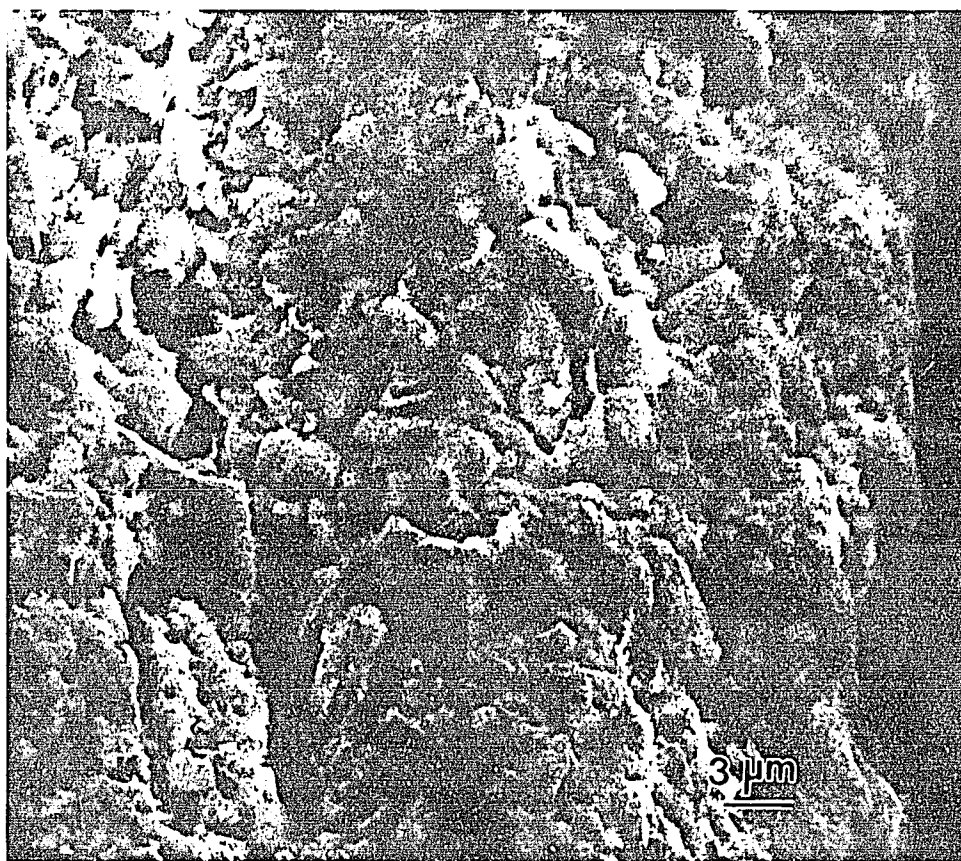


Figure 18. SEM cross-section micrograph of a bulk sample #2. It showed that the BC treatment affected the surface of sample to a depth of about 10 μm .

one unexposed piece and another exposed piece, which both were from the same sample, were observed side by side at the same working conditions such as same magnification, etc. Before exposure in the ballistic compressor, the compositions of the thin samples of Bi-Pb-Sr-Ca-Cu-O compounds vary greatly from one location to another. For example, the ratio of characteristic x-ray peak intensities of Cu to (Bi+Pb) ranges from 0.2 to 0.4 depending on the location in the sample. The ratio of characteristic x-ray peak intensities of Sr : Ca ranges from 1.9 to 1.5. Pb and Bi intensities are very difficult to estimate separately, for their peaks in the low energy region are overlapped because of having close energies of 2.342 Kev and 2.418 Kev, respectively. It should be noted that the superconducting phases have a variable composition in a Bi solid solution (39). After the BC treatment, no straightforward relationship can be obtained between the unexposed and exposed samples, so that means the contents of Bi, Ca, and Sr changed randomly. No obvious regularity in the average composition was obtained although great attention was paid to take a series of average composition analyses from the exposed surface. But most EDS data show that the content of copper increased after the BC treatment. The qualitative cross-sectional composition analysis of thin samples showed clear changes in contents of oxygen and Cu after the BC treatment. Figure 19 shows a cross-sectional micrograph of the sample thin#2 after the third BC treatment.

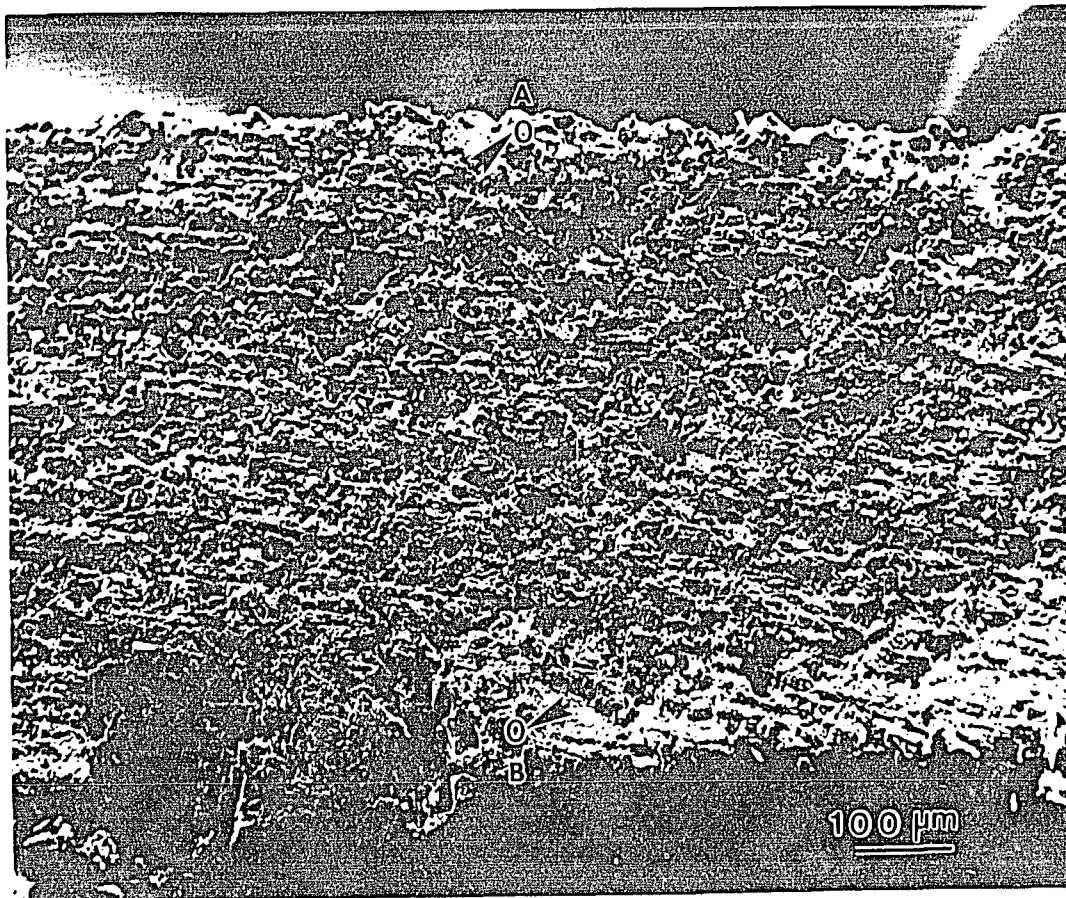


Figure 19. SEM cross-section micrograph of the pellet thin#2.

The point analysis was carried out at the points which were less than 10 μm from the unexposed surface (arrowed point A) and from the exposed surface (arrowed point B) on the cross-section of the thin sample.

Figure 20 (a) and (b) illustrate typical energy dispersive spectra which are from the A and B points in Figure 19, respectively. Comparison of these two spectra shows that the ratio of $\text{Cu}_{\text{K}\alpha}$ to Bi increased from 0.27 to 0.52.

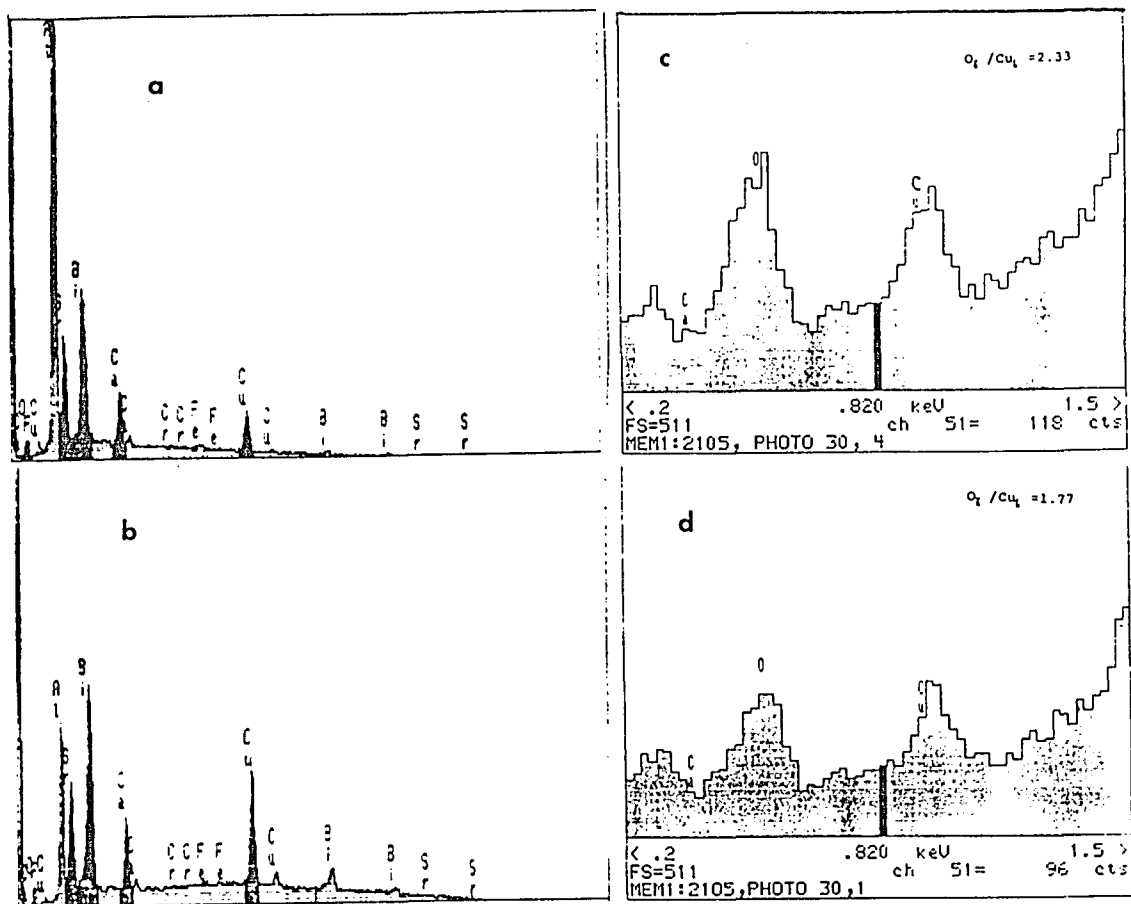


Figure 20. EDS data from near the unexposed and exposed edges of the sample Thin#2. (a) was from point A in Figure 19, which was very near the unexposed edge of the sample thin#2, and (b) was from point B which was very near the exposed edge. (c) and (d) are the expanded low energy regions in (a) and (b), respectively.

The aluminum peak originates from the specimen holder. Especially, the comparison of the ratio of $O_{K\alpha}$ to $Cu_{L\alpha}$, which have similar energies, shows a very interesting result in Figure 20 (c) and (d), which correspond to the unexposed and exposed sides, respectively. This result shows that the amount of oxygen decreased after exposure in the ballistic

compressor. It appears that oxygen evaporated in the BC treatment process. After examining several points on each side of the sample thin#2, we found the general tendency that the ratio of $\text{Cu}_{K\alpha}$ to Bi is slightly higher on the exposed side and the amount of oxygen decreased after the BC treatment. These results are shown in Table IV. But the fourth trial shows opposite results. This may be due to the fact that this point analysis was too far from the exposed side. We could not quantify exactly the oxygen loss because a standard of known oxygen content was not available.

TABLE IV

COMPARISON OF THE RATIO OF $\text{Cu}_{K\alpha}$ TO Bi AND THE RATIO OF $\text{O}_{K\alpha}$ TO $\text{Cu}_{L\alpha}$ BEFORE AND AFTER BC TREATMENT

Trial	$\text{Cu}_{K\alpha}/\text{Bi}$		$\text{O}_{K\alpha}/\text{Cu}_{L\alpha}$	
	unexp.	exp.	unexp.	exp.
1	0.16	0.26	2.89	1.17
2	0.21	0.43	2.30	1.53
3	0.18	0.32	2.31	1.24
4	0.25	0.18	2.07	2.35

X-ray Diffraction Investigation

X-ray diffraction has been used to detect the presence or absence of the three superconducting phases of Bi compounds by observing the diffraction patterns obtained by standard x-ray diffraction analysis methods. The phase identifications were made by using the known lattice parameters for the

tetragonal structures of these three phases, which were published by Tallon et al.(43) and Maeda et al.(92). The distance d_{hkl} between adjacent lattice planes in the space lattices is expressed as follows:

$$\frac{1}{d_{hkl}^2} = \frac{h^2 + k^2}{a^2} + \frac{l^2}{c^2} \quad (4.1)$$

where the h, k, l are the Miller indices of the respective plane and a and c are the lattice parameters. The lattice parameters for the three phases are shown in Table V (43).

TABLE V
LATTICE PARAMETERS OF THREE PHASES IN Bi-BASED SYSTEM

	a (Å)	b (Å)	c (Å)
n=1 (2201)	5.4	5.4	24.6
n=2 (2212)	5.4	5.4	30.76
n=3 (2223)	5.4	5.4	37.1

These three phases in the sample were identified by comparing the spectra with a computer program (93), which computed a series of theoretical values of d-spacing (d_{cal}) of the planes, which were obtained by using the known lattice parameters for the three phases in Bi-based compounds. Thin samples and thin film samples were investigated under an x-ray diffractometer before and after each exposure in the ballistic compressor. Penetration depth of x-ray was about one thousand unit cells.

It is thought that the changes in the relative intensities and the full-width-half-maximum (FWHM) values for the same peaks were caused by the BC treatment.

The x-ray diffraction patterns of the sample thin#2 before and after exposure in the ballistic compressor are shown in Figure 21. As is well known (94-96), the diffraction line at low 2θ region such as $2^\circ < 2\theta < 25^\circ$ are clean signals with less overlap from other peaks. For example, the diffraction peak at $2\theta = 7.2^\circ$ corresponding to (002) planes of the 2201 phase, the line at $2\theta = 5.7^\circ$ corresponding to (002) planes of the 2212 phase, and the line at $2\theta = 4.7^\circ$ corresponding to (002) planes of the 2223 phase are easily distinguishable. So these are examined carefully to indicate best the relative amounts of the superconducting phases. In the high 2θ region, the diffraction lines are often overlapped, and therefore it is difficult to calculate the contribution of each individual phase. As such, these two diffraction patterns for the sample thin#2 in Figure 21 (a) and (b) reveal the absence of the peak at $2\theta = 7.2^\circ$ corresponding to the 2201 phase and the peak at 4.7° corresponding to the 2223 phase for both before and after the BC treatment. A broad peak at 21.8° corresponding to the 2201 phase disappeared after exposure to hot, dense argon. But the amount of the 2212 phase obviously increased because the intensity of the peak at $2\theta = 5.8^\circ$ corresponding to the 2212 phase increased after the BC treatment, as is shown in Figure

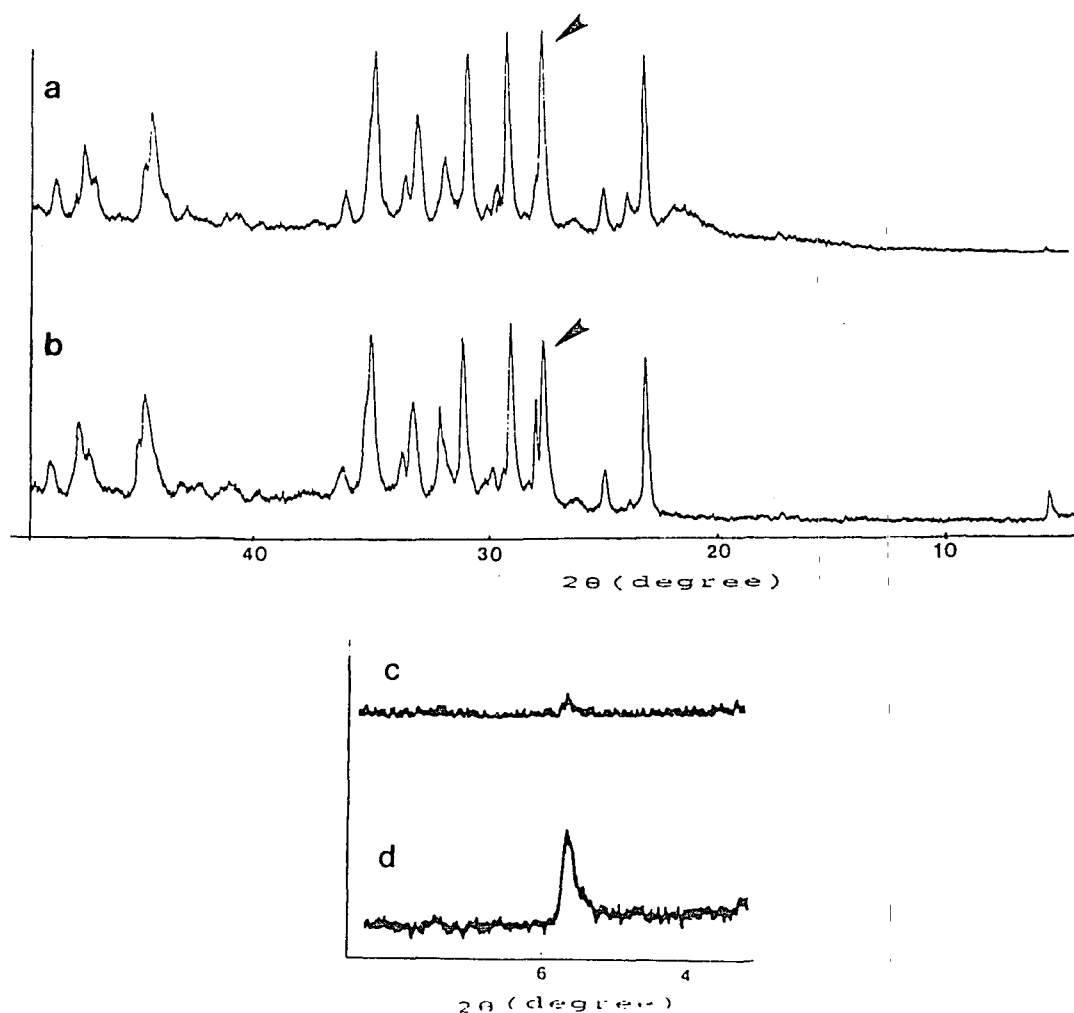


Figure 21. The Cu K_α x-ray diffraction pattern of sample thin#2. (a) before and (b) after the first exposure in the ballistic compressor. X-ray diffractographs from (a) and (b) in the low angle region of (c) before and (d) after the BC treatment. The arrowed peak was unidentified.

21 (c) and (d). The new peak at $2\theta = 27.8^\circ$ (arrowed in Figure 21) was unidentified.

Identification of all the major reflections indicated that the sample contained mainly the 2212 phase, which also

coexists with other minor phases, including the 2223 phase and the 2201 phase. In the case of the sample thin#2 the first 18 lines were taken into account and shown in Table VI, in which the main reflection were indexed. Here the theoretical d-spacing d_{cal} and the experimental d_{obs} were compared. Additionally, the relative intensities and the FWHM of each peak were evaluated.

From comparison, there are no changes in the locations of peaks before and after exposure. This indicates that the geometry of the lattice was not affect by the BC treatment, and the deviation of 0.1° between before and after treatment is within the error range for the diffractometer measurements. In the high angle region, the changes of the relative intensities for these three phases did not show clearly the growth of one phase with the decrease of another phase. The full-width-half-maximum measurements are either related to the size of crystals (97), or are the result of stacking faults, etc (42). In Table VI, the FWHM of the main reflections, for which the relative intensities of peaks are higher than 50%, increased after the BC treatment. These lines which broadened mainly correspond to the 2212 phase.

For comparison, the x-ray diffraction data for the sample thin#1 are given in Table VII. In the low angle region, the peak at $2\theta = 5.7^\circ$ corresponding to the 2212 phase did not change after the BC treatment, but a clean peak at $2\theta = 24.6^\circ$ corresponding to (105) plane for the low- T_c phase

disappeared, and two new peaks appeared after the first BC exposure at $2\theta=24.0^\circ$ and $2\theta=24.9^\circ$. These are indexed as the (113) plane for the 2212 phase and the (0010) plane for the 2223 phase, respectively, without ambiguity. These features are also shown in the x-ray diffractographs for the sample thin#1 in Figure 22.

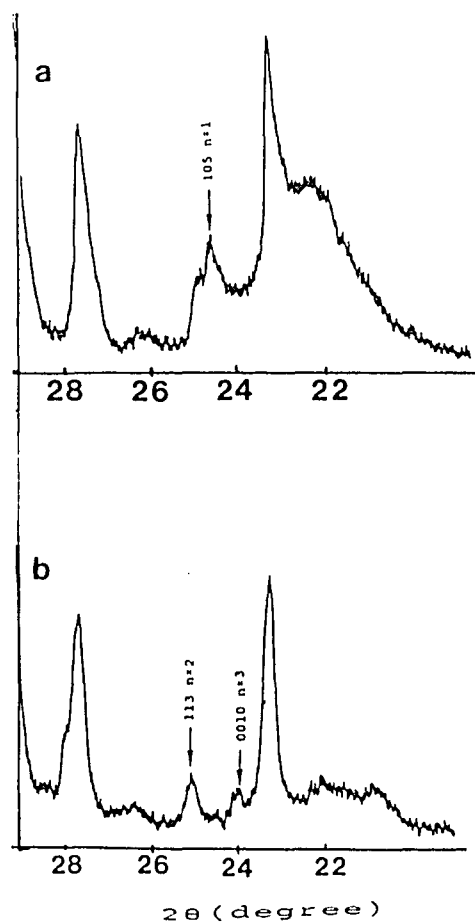


Figure 22. In low angle region, x-ray diffractographs for the sample thin#1. (a) before and (b) after first exposure in the ballistic compressor.

In Table VII, a point of similarity between the samples thin#1 and thin#2 is that the effect on the relative intensities of lines for a certain phase, which could be changed by the BC treatment, was not clearly evident in the high angle region. Appositely, the FWHM data shows a tendency to decrease for the lines with higher relative intensities than 50, instead of an increase for the sample thin#2 after the BC treatment, which is shown in Table VI. The results of the FWHM obtained in the x-ray experiments is similar to that of Straub (86), who found also opposite results for two thin samples.

Table VIII shows the x-ray diffraction data for the thin film sample film#3. Only six reflection lines were obtained in x-ray diffraction patterns. From comparison, similar increases of the relative intensities of lines in the low angle region and similar increases of the FWHM of peaks were observed after the second exposure in the ballistic compressor.

However, some additional lines which were not explained by the presence of the three phases mentioned above might be caused by some small contribution to the composition of sample by compounds such as CaCu_2O_3 ($2\theta=36.3^\circ$), Ca_2PbO_4 ($2\theta=17.6^\circ$), etc., similar to the results reported by Tu, *et al.* (77) and Jhu *et al.* (96).

TABLE VI
X-RAY DIFFRACTION DATA FOR SAMPLE THIN#2 BEFORE
AND AFTER THE SECOND EXPOSURE IN THE
BALLISTIC COMPRESSOR

$2\theta_{\text{obs}}$ (degree)		h k l	n	d_{cal} (Å)	d_{obs} (Å)		$I/I_{\text{o obs}}$		FWHM (degree)	
$2\theta_{\text{un}}$	$2\theta_{\text{exp}}$				d_{un}	d_{exp}	unexp	exp	unexp	exp
5.7	5.7	0 0 2	2	15.38	15.38	15.38	2	16	0.13	0.24
21.8	0	0 0 6	1	4.07	4.07	0.0	12	0	1.3	0.0
23.1	23.1	0 0 8	2	3.85	3.85	3.85	87	95	0.26	0.32
23.9	23.8	1 0 6	2	3.72	3.71	3.73	19	8	0.4	0.30
24.9	24.8	1 1 3	2	3.58	3.58	3.58	24	25	0.36	0.30
27.5	27.5	1 1 5	2	3.24	3.24	3.24	100	99	0.34	0.38
27.8	27.8	*	*	*	3.21	3.21	21	52	*	0.18
28.9	29.0	0 0 10	2	3.09	3.09	3.08	95	100	0.3	0.28
29.8	29.8	1 1 5	1	3.00	3.01	3.01	17	14	0.28	0.4
31.0	31.0	1 1 7	2	2.88	2.88	2.88	86	98	0.36	0.36
32.0	32.0	1 1 9	3	2.79	2.80	2.80	32	55	0.52	0.4
33.2	33.1	2 0 0 2 0 0 2 0 0	1 2 3	2.70	2.70	2.70	55	58	0.4	0.5
33.7	33.6	0 2 2	2	2.66	2.66	2.66	21	22	0.4	0.4
34.9	34.9	0 0 12	2	2.57	2.56	2.56	87	96	0.52	0.52

TABLE VI
X-RAY DIFFRACTION DATA FOR SAMPLE THIN#2 BEFORE
AND AFTER THE SECOND EXPOSURE IN THE
BALLISTIC COMPRESSOR
(continued)

$2\theta_{\text{obs}}$ (degree)		h k l	n	d_{cal} (Å)	d_{obs} (Å)		I/I_o obs		FWHM (degree)	
$2\theta_{\text{un}}$	$2\theta_{\text{exp}}$				d_{un}	d_{exp}	unexp	exp	unexp	exp
44.7	44.6	2 0 10	2	2.03	2.03	2.03	56	53	0.52	1.04
45.0	44.9	1 2 10	3	2.01	2.02	2.02	31	36	*	*
47.2	47.2	1 0 18	3	1.92	1.92	1.92	24	27	*	*
47.7	47.7	2 2 0 2 2 0 2 2 0	1 2 3	1.91	1.91	1.91	40	44	0.52	0.48

* The peak could not be evaluated the full-width-half-maximum value because of its broadening.

* It is difficult to index the peak.

obs = observed value
cal = calculated value
un = unexposed in the BC
exp = exposed in the BC

TABLE VII
X-RAY DIFFRACTION DATA FOR SAMPLE THIN#1
BEFORE AND AFTER THE SECOND EXPOSURE IN THE
BALLISTIC COMPRESSOR

$2\theta_{\text{obs}}$ (degree)	h k l	n	d_{cal} (Å)	d_{obs} (Å)		I/I_0 obs		FWHM (degree)	
$2\theta_{\text{un}}$				d_{un}	d_{exp}	unexp	exp	unexp	exp
5.7	0 0 2	2	15.38	15.38	15.38	12	12	0.3	0.2
22.1	1 0 5	2	4.05	4.04	4.04	7	10	0.3	0.2
23.1	0 0 8	2	3.85	3.85	3.85	79	85	0.3	0.3
0	1 1 2	2	3.71	0	3.71	0	10	0	0.2
24.6	1 0 5	1	3.62	3.62	0	21	0	0.2	0
*	1 1 3	2	3.58	*	3.57	*	19	*	0.3
27.6	1 1 4	1	3.24	3.23	3.23	83	73	0.4	0.4
29.0	0 0 10	2	3.08	3.08	3.07	90	98	0.5	0.3
29.8	1 1 5	1	3.00	3.00	2.98	16	23	0.3	0.15
31.0	1 1 7	2	2.88	2.88	2.87	83	73	0.3	0.4
32.0	1 1 9	3	2.79	2.79	2.79	34	41	0.5	0.4
33.2	2 0 0 2 0 0 2 0 0	1 2 3	2.70	2.70	2.69	52	44	0.5	0.3
35.0	0 0 12	2	2.55	2.56	2.55	100	100	0.6	0.6
44.6	0 2 10	2	2.03	2.03	2.03	72	63	0.9	1.0

TABLE VII

X-RAY DIFFRACTION DATA FOR SAMPLE THIN#1
BEFORE AND AFTER THE SECOND EXPOSURE IN THE
BALLISTIC COMPRESSOR
(continued)

$2\theta_{\text{obs}}$ (degree)		h k l	n	d_{cal} (Å)	d_{obs} (Å)		I/I_0 obs		FWHM (degree)	
$2\theta_{\text{un}}$	$2\theta_{\text{exp}}$				d_{un}	d_{exp}	unexp	exp	unexp	exp
47.3	47.3	1 0 18	3	1.91	1.91	1.91	7	20	0.1	0.3
47.6	47.7	2 2 0 2 2 0 2 2 0	1 2 3	1.90	1.90	1.90	29	27	0.3	0.3
49.0	49.1	2 0 12	2	1.86	1.86	1.85	24	19	0.6	0.6
50.5	50.5	1 1 15	2	1.80	1.81	1.81	62	61	0.45	0.45

TABLE VIII

X-RAY DIFFRACTION DATA FOR THIN FILM SAMPLE FILM#3
BEFORE THE FIRST AND AFTER THE SECOND EXPOSURE
IN THE BALLISTIC COMPRESSOR

$2\theta_{\text{obs}}$ (degree)	$2\theta_{\text{un}}$	$2\theta_{\text{exp}}$	h k l	n	d_{cal} (Å)	d_{obs} (Å)		I/I_0 obs		FWHM (degree)	
						d_{un}	d_{exp}	unexp	exp	unexp	exp
5.8		5.8	0 0 2	2	15.38	15.23	15.23	0	3	0	0.18
23.2		23.2	0 0 8	2	3.80	3.83	3.83	93	86	0.24	0.22
29.1		29.1	0 0 10	2	3.08	3.07	3.07	100	100	0.22	0.22
35.1		35.1	0 0 12	2	2.54	2.55	2.55	56	57	0.24	0.38
47.3		47.2	1 0 18	3	1.91	1.92	1.92	22	24	0.22	0.56
60.4		60.4	2 2 12	2	1.53	1.53	1.53	26	19	0.26	0.36

TEM Investigation

Two selected area ($1.8 \times 10^{-5} \text{ cm}^2$) electron diffraction patterns with an incident beam along [001] for the bulk sample #2 before and after the first exposure in the ballistic compressor are shown in Figure 23 (87).

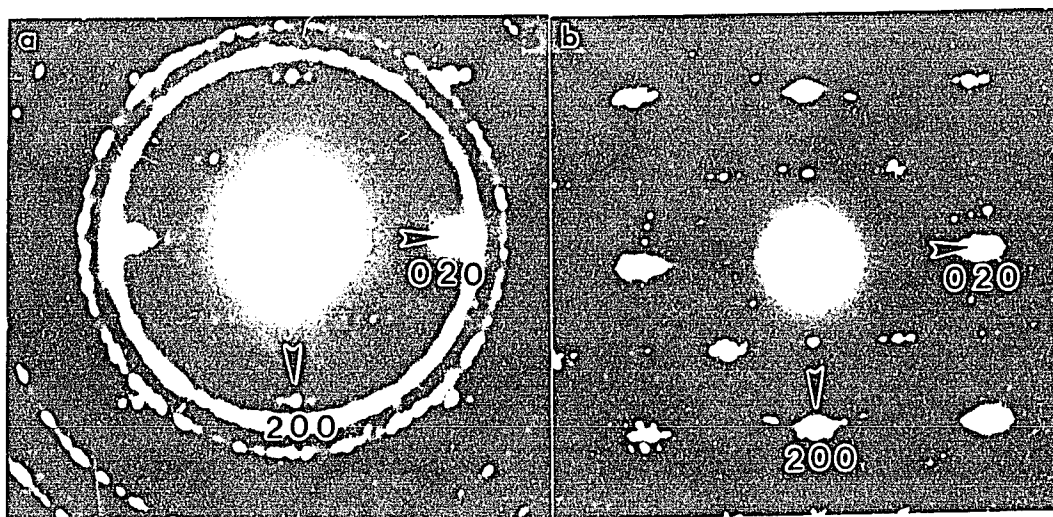


Figure 23. Typical electron diffraction pattern from the bulk sample #2 along the [001] direction. (a) before and (b) after the BC treatment.

These two electron diffraction patterns (a) and (b) in Figure 23 were obtained from particles removed from the surfaces of sample before and after the first BC treatment, respectively. The rings in this pattern (Figure 23 (a)) were from a calibration gold film, which was deposited on the same grid. Comparison of these two electron diffraction patterns indicate that the relative intensities changed after the first treatment. For example, before exposure in the ballistic

compressor, spots along the $[100]$ direction show equal intensities, in Figure 23 (a). After the BC treatment, spots along this direction showed unequal intensities (Figure 23 (b)), similar results were observed in the sample thin#1 and

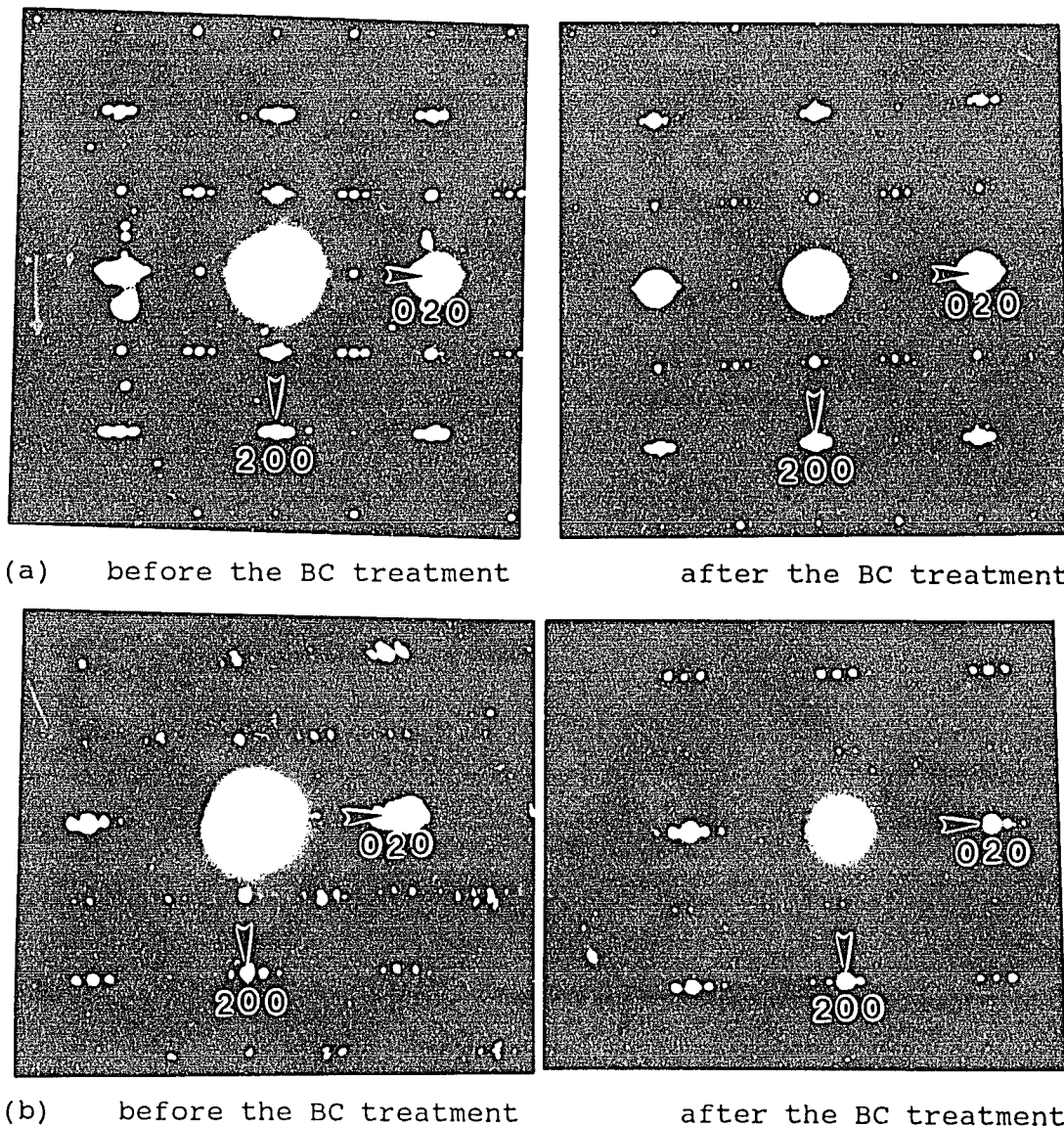


Figure 24. Typical electron diffraction pattern along the $[001]$ direction. (a) from the sample thin#2 and (b) from the thin film sample film#1.

in the thin film samples film#3, which are shown in Figure 24 (a) and (b), respectively.

The lattice constants of the superconductors illustrated in these patterns were calculated, yielding a pseudo-tetragonal cell of $a \approx b = 5.4 \text{ \AA}$. Values of c for the three phases in Bi-based compounds were reported elsewhere by other research groups (89-91). A common, important feature of the electron diffraction patterns of Bi-based compounds is a fall-off of intensity of reflections between fundamental reflections along $[010]$ and an incommensuration of the superlattice reflections along the same direction (89). The lattice constant of the superstructure observed between two adjacent spots was measured carefully under a travelling microscope. For example, along a line of strong spots in Figure 23 (a) and (b), the main reflections (200, 020, and so forth) are flanked by two or three weak spots on each side with a main separation of 25.4 \AA between the secondary spots, which is the same as in other reports (67,92,94). This is consistent along the pattern and corresponds to the incommensuration with a $4.7 \times b \text{ \AA}$ period along the b axis. Electron diffraction patterns of the thin film sample film#3 before and after the third BC treatment are shown in Figure 25 (a) and (c), in which the strong modulation along the b -direction is observed clearly. The important point to notice is that the intensities of the main reflection 020 spots along the lines A in Figure 25 (a) and (c) increased after the BC

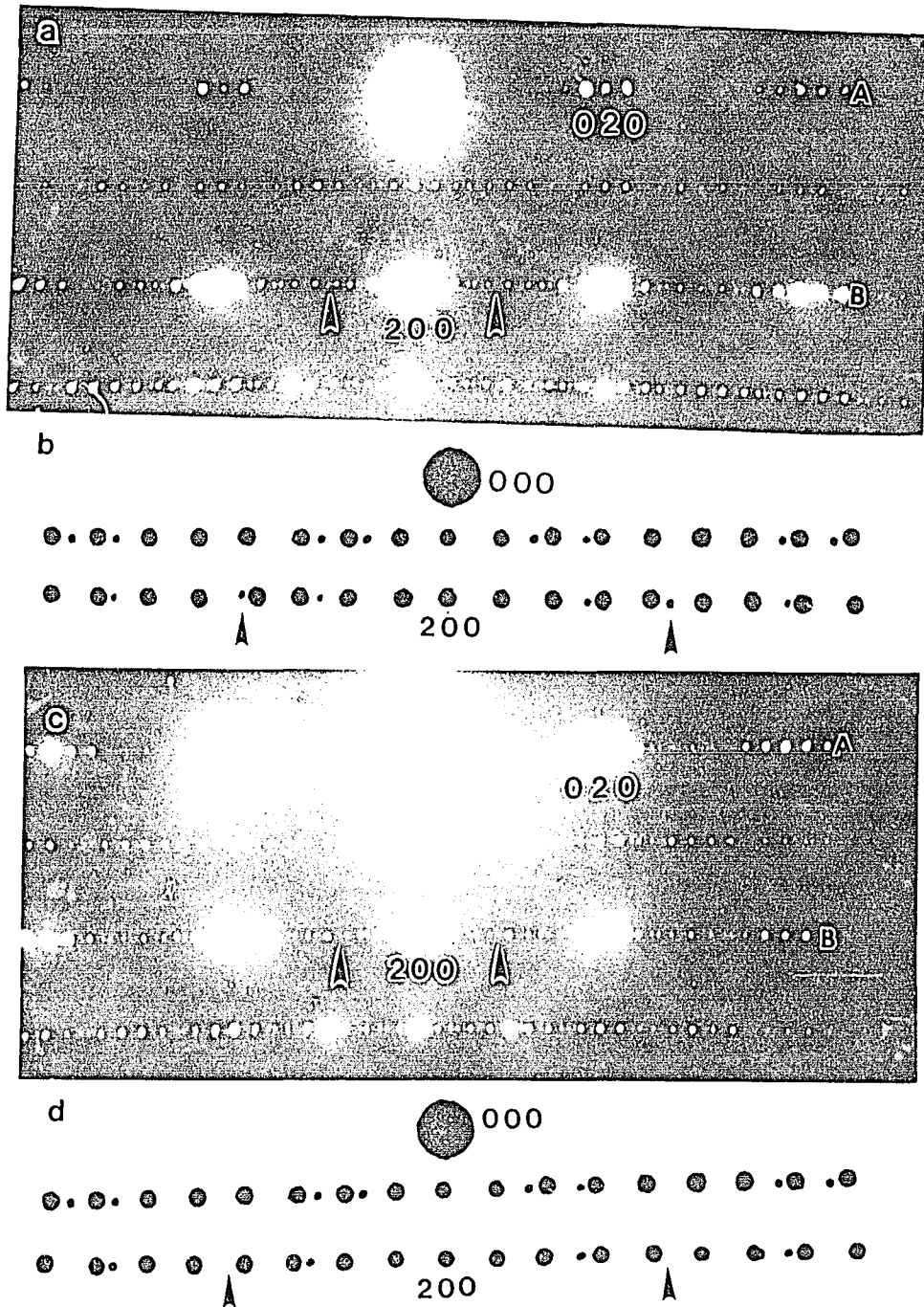


Figure 25. Selected area electron diffraction patterns from a thin film sample film#3 in the $[001]$ zone axes. (a) before and (c) after the third BC treatment. (b) and (d) Schematic diagrams of the superstructure in the a-b plane before and after the third BC treatment.

treatment, but inversely, the intensities of the main reflection 200 spots along the lines B decreased after this treatment. In Figure 25 (a) and (c), the periodicities of the superlattice are complicated and composed of approximate periodic combinations. Although the periodicity of 25.4 Å is present, additional periods of 38.7 Å and 72.6 Å (indicated by arrows in Figure 25) are also observed. This superstructure is shown schematically in Figure 25 (b) and (d). The intensities of the spots which correspond to an interplanar distance of 72.6 Å are weaker than the rest of the spots. R. Herrera *et al.* (89) reported the periods of 26.4 Å, 27.2 Å, 27.5 Å, and 30.9 Å. E. Hewat *et al.* (91) found average repeat periods of 25.1 Å, 25.5 Å, 75.2 Å, and 102 Å.

In Figure 25 (a) and (c), a comparison between these two electron diffraction patterns, which were observed carefully with a travelling microscope, shows that BC treatment leads to a change in the type of modulation. A series of notable weak spots are arrowed in Figure 25 (a) and (b). These correspond to the superstructure length of 72.6 Å in the unexposed sample, whereas these weak spots disappeared after the BC treatment in Figure 25 (c) and (d). This is an interesting phenomenon but not understood.

Twist boundaries, which occur in bands of parallel planes within a crystal, were reported in Bi-based compounds (91). Figure 26 (a) shows the electron diffraction pattern of a twist boundary from the edge of a particle of the thin film

sample film#1 (Figure 26 (b)) after the first BC treatment. Viewed down the c-axis, the successive layers have the a- and b-axes interchanged. The twist boundary plane is on (001).

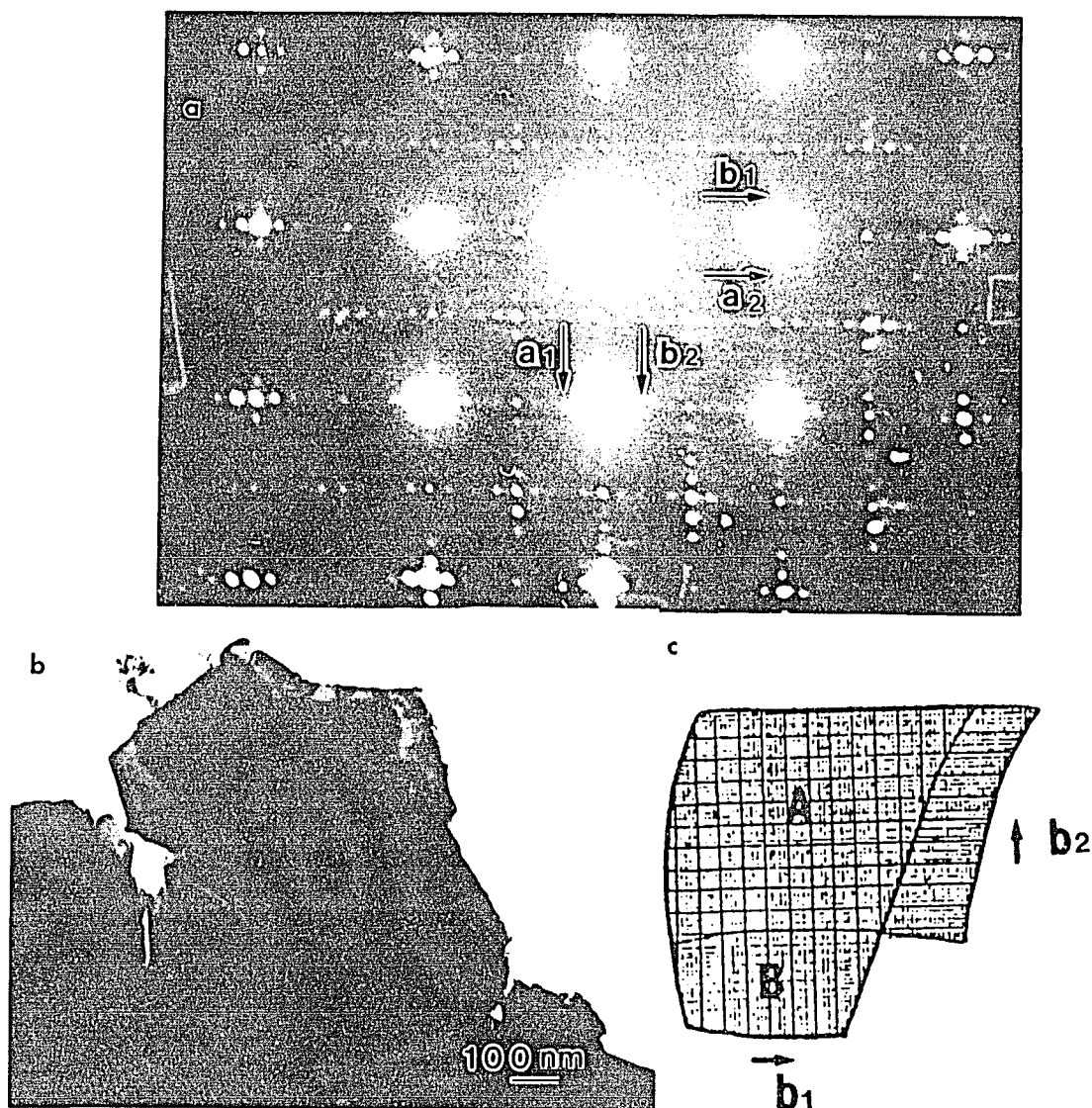


Figure 26. Electron diffraction pattern of a twist boundary ((001) plane) for film sample film#1 found after the first BC treatment. (a) EDP of the twist boundary. (b) EDP from the edge of a particle of the exposed sample film#1. (c) Schematic representation of a twist boundary viewed down [001].

This type of defect is often associated with overlapping crystals, which are shown schematically in Figure 26 (c). The other type of twist electron diffraction pattern from the same sample film#1 after exposure in the ballistic compressor is shown in Figure 27 (a).

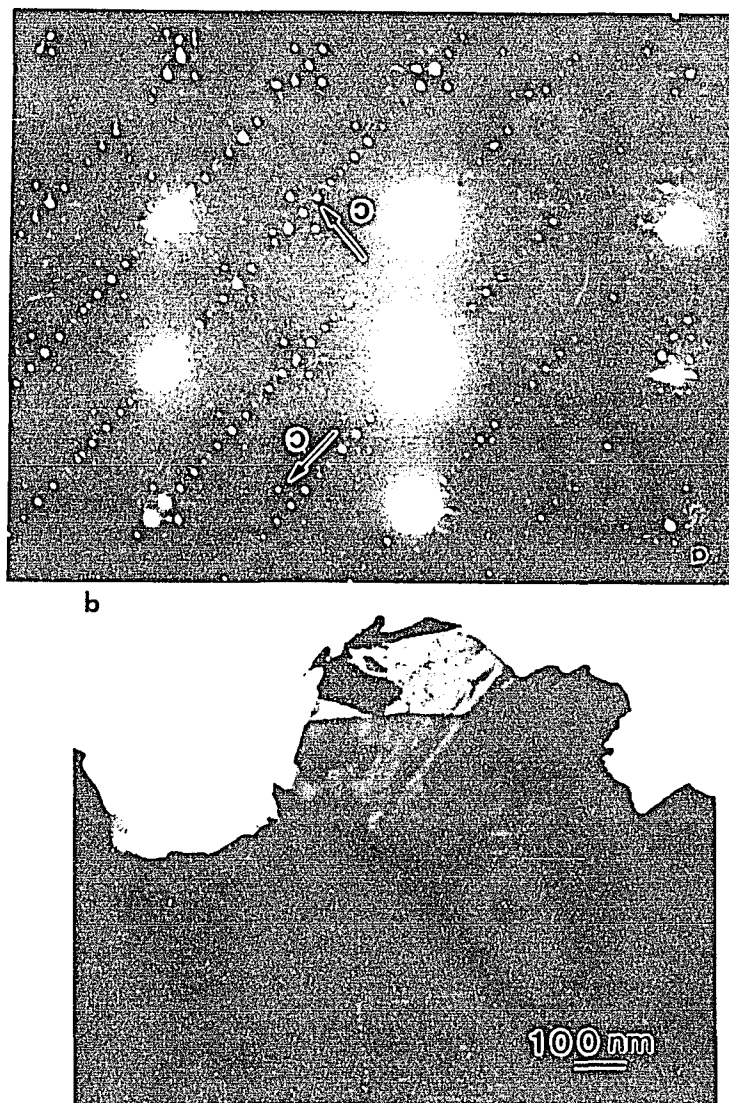


Figure 27. Electron diffraction pattern ((010) plane of a twist boundary found in the same sample film#1. (a) EDP of the twist boundary. (b) EDP from the edge of a particle of the exposed sample.

This electron diffraction pattern is along the [010] zone and the successive layers are overlapped at 81° . Similar twist electron diffraction patterns were found in the exposed thin samples. The density of twist boundaries seen in the exposed samples is higher than in the unexposed samples. The BC treatment apparently caused this increase.

DISCUSSION

The samples used for studying the effect on composition, structure, and superconductivity in the Bi system after exposure in the ballistic compressor have revealed many interesting results. The electrical resistance versus temperature measurements for all samples mentioned above show that the T_c increased about 3 K - 6 K after exposure in the ballistic compressor. Sample #2 exhibited a T_c of 85 K and 89 K before and after the first BC treatment, respectively, whereas, the superconducting transition width changed from 18 K before exposure to 12 K after the second exposure.

More than one high T_c phases exist in the samples studied. These have showed different onset temperatures. After exposure in the ballistic compressor, a common phenomenon is that the R-T curves showed two different slopes. For the bulk sample #2, only one superconducting transition was observed, but two transitions occur in the samples #1, thin#1, and thin#2, indicating the presence of two high T_c phases. This phenomena indicates that there is a change from

the low T_c phase to the high T_c phases during the BC treatment. Worth mentioning is that the electrical resistance versus temperature measurements for the bulk and thin samples showed a variation in T_c as measured at different directions on the samples, which was reported very clearly by Straub (86) also. This phenomenon was probably due to the inhomogeneity of the cuprate superconductors. But the susceptibility measurements determined the overall superconducting behavior of the whole sample (including the substrate but its magnetic susceptibility was so small that would not affect this measurement). The susceptibility versus temperature measurements for the sample thin#2 show that the onset temperature of samples after BC treatment remained unchanged at 113 K. And the onset temperatures for the thin film samples film#1 and film#3 after the BC treatment were higher than before this treatment, thus seeming to improve the superconducting behavior with an increase of about 3 K after exposure in the ballistic compressor. The likelihood is that the BC treatment is a surface effect, and thin pellet samples have much larger masses than the thin film samples. The amount of 2223 phase formed on the surface by BC treatment is too small to strongly influence the susceptibility of the bulk sample. So, it is difficult to show a change in the onset temperature by means of susceptibility measurements. But, the susceptibility versus temperature and R-T plots for a thin pellet sample are quite identical in showing a sharp change in

the slope at 113 K after exposure of a sample in the ballistic compressor. The diamagnetic signal is not smooth after BC treatment, but contains steps in the region between about 113 K and 77 K. This indicates also the presence of more than one high T_c phase after the BC treatment. Further exposure (more than three) in the ballistic compressor caused the samples to break.

These experimental results of the resistance and susceptibility measurements for the same kind of samples show a variation of range in T_c after exposure in the BC. And, the reproducibility of resistance measurement for some samples remains a problem. This problem may be caused by the inhomogeneity of samples. The samples were not treated uniformly in the BC process, as was obvious under SEM examination. However, it has been seen that the improvement of superconducting behavior and the presence of more high- T_c phases indicates an important possibility of improved superconducting properties by transformation in the BC treatment process.

X-ray diffraction patterns of samples thin#1, thin#2, and film#3 were examined for the superconducting phases and for impurity phases and compared to the published structures. All samples tested were multiphase, containing mostly 2212 phase, and minor fractions of 2201 phase and 2223 phase. The high T_c phase has been detected in the high angle region of x-ray diffraction pattern. Its presence was also suggested by

the results of magnetic susceptibility and electrical resistance measurements. Ganapathi *et al.* (98) and Polonka (99) reported the same phenomenon for the x-ray data and the susceptibility measurements. The volume percent of high T_c phase was estimated to be less than 5% (98, 99), which is the detection limit of the x-ray diffractometer, since it was not observed in the x-ray diffraction patterns. The close examination of x-ray diffraction patterns of samples thin#2 and film#3 suggests that the 2212 phase at $2\theta = 5.7^\circ$ is increased in appreciable amount, and the intensity for the low T_c phase decreases after exposure of sample in the ballistic compressor. Similar phenomena are displayed in the x-ray diffraction pattern of the exposed sample thin#1; the line at $2\theta = 24.6^\circ$ due to the low T_c phase decreased in intensity below the background level, while the peaks due to 2212 and 2223 phases increased and were detectable, probably due to phase transformation taking place during the BC treatment. Therefore, these x-ray observations also support the conclusion drawn from the resistance and susceptibility measurements that indicate improvement of superconducting behavior and phase transformation.

Table VI , VII, and VIII all show changes in the relative intensities for the tested samples, with especially, an increase in the intensities of the higher peaks of the 2212 phase. The changes of relative intensities for both x-ray diffraction data and the electron diffraction patterns after

the exposure of samples in the ballistic compressor may be due to: (1) change in relative amounts of phases present, and (2) change in the arrangement of atoms in structures of the cuprate superconductors (100), and (3) a small change in the orientation of sample. In the x-ray diffraction and electron diffraction experiments, the intensity of the scattered wave from the unit cell of samples, I_{hkl} , is proportional to the square of the amplitude of the wave (101). Hence,

$$I_{hkl} \propto |F(hkl)|^2 \quad (4.2)$$

where $F(hkl)$ is the structure factor, which expresses the combined scattering wave from the hkl plane in the unit cell. The resultant wave for the unit cell is therefore

$$F(hkl) = \sum_{j=1}^N g_j \exp(i\phi_j) \quad (4.3)$$

here g_j and ϕ_j are the amplitude and phase factors of the atomic scattering wave in this unit cell. The x-ray and electron diffraction data described above show that the geometry of the unit cell did not change after BC treatment because of the unchanging nature of both locations of the peaks in the XRD and the main reflection spots in the EDP. From the intensity expressions, the intensities of the Bragg reflection depend on the type and the arrangement of atoms at

each lattice point in the unit cell.

X-ray diffraction data for the exposed sample film#3 shows an increase in the FWHM compared with the unexposed sample. X-ray diffraction line broadening is a very complex phenomenon. Bartram (97) and Klug (102) analyzed this phenomenon clearly. They concluded that the combined effects of a number of instrumental and physical factors, e.g. x-ray source profile corresponding to the instrument, smaller crystalline size, crystal imperfections such as twinning, composition inhomogeneity, etc., contribute to line breadth.

In 1918, P. Scherrer (103) determined the relationship between crystallite size and x-ray line broadening as follows:

$$D = \frac{K\lambda}{\beta \cos \theta} \quad (4.4)$$

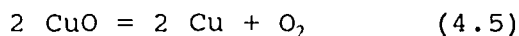
where D is the average crystallite size, λ is the wavelength, θ is the Bragg angle, β is the angular width at half-maximum intensity of the pure diffraction line on the 2θ scale, and K, which depends on the crystallite shape, is a constant approximately equal to unity. From this equation, the crystallite size can be calculated, but the major premise of the x-ray line broadening method to the crystallite size determination should be strictly applied to materials which do not contain any defects (97). It should be noted that there is little change in relative intensity of the (0012), (1018) and (2212) diffraction lines after two BC exposures (Table

VIII), but there is significant broadening of these lines. This suggests that the BC exposure had only a minor effect on the amount of the $n = 2$ and $n = 3$ phases. The main effect of BC exposure may have been caused by the increase in the concentration of crystal defects due to change in composition caused by rapid evaporation of elements such as oxygen. Löscher *et al.* (100) and Tarascon *et al.* (42) suggested that the broadened x-ray reflections demonstrate the presence of stacking faults in the tested sample. A type of stacking fault, twist boundary, was deduced from electron diffraction patterns of the samples after exposure in the ballistic compressor.

SEM surface microstructure of the high T_c cuprate superconductor samples before the BC treatment show the presence of the plate-like grains, which probably have their thickness dimension parallel to the c-direction. The samples also contained needle-like and columnar grains. Such a microstructure suggests that the very thin plate crystallites, which correspond to the high T_c phase, are piled up and weakly connected to each other in the samples. From the analytical results of the EDS, the columnar grains contained Sr, Ca and Cu, which was also reported elsewhere (99), and the needle-like grains were considered to be amorphous (104). This may indicate that the material had not been completely reacted. It has been observed by Kikuchi *et al.* (105) and Shi *et al.* (106) that the size of the plate-like grains increased

gradually with increases in the sintering temperature and time. After exposure of samples in the ballistic compressor, the plate-like grains still remained on the surface that was not apparently melted, but it was difficult to find differences in the size of plate-like grains. Furthermore, a portion of the surface was melted, and porous structure occurred after the BC treatment. It seems likely that the molten state followed by rapid cooling results in a finely crystallized high- T_c phase.

The ballistic compressor treatment process is an open system, that is, chemical elements contained in the samples, especially oxygen, are readily lost from the system. When the sample is exposed to hot, dense argon gas in the ballistic compressor, temperature and pressure are raised in a very short time, so Bi, Sr, Ca, Cu, and oxygen may be vaporized readily, depending on their individual vapor pressures. The BC treatment also changed the black color of the surface of the Bi-based superconductor sample to a dark red color, which is rather like the color of copper. This is possibly due to oxygen loss as follows:



This conclusion is supported strongly by the EDS investigations. After the BC treatment, the EDS data that were from the surface of samples at low magnification showed

that no consistency in the average composition was obtained. Especially, the contents of Bi, Ca, Sr and Cu changed randomly. The possible explanation may be that the chemical content changed randomly. Furthermore, at high magnification, comparison of the EDS analysis between the inside and the outside of a pore that was formed by the BC treatment showed that the content of copper obviously increased. The point EDS investigations that were from the cross sections of samples showed that there was an increase in the content of Cu. Of more importance is the fact that the ratio of the oxygen K α line intensity to the Cu L α line intensity decreased after exposure of the sample in the ballistic compressor. This further demonstrates that oxygen loss occurred in the BC treatment process.

The variation of oxygen content in the sample is of great interest in the oxide superconductors. According to rather precise experiments (107), it is established that the oxygen content of the cuprate superconducting compounds is the principal variable affecting T_c . For the Bi-based superconductors, the oxygen content decreases with an increase of T_c , which is opposite to the effect of oxygen stoichiometry on T_c observed in the $\text{YBa}_2\text{Cu}_3\text{O}_y$ and $\text{La}_2\text{CuO}_{4+x}$ compounds. Zhao et al. (107) has found that T_c increased about 25 K corresponding to a weight loss of 0.16% (corresponding to a change of 0.09 oxygen per formula unit), which was believed due to the oxygen loss, because the weight loss only occurs by changing the

quenching temperature without observable structural change appearing in the XRD patterns. Zhao (108) also reported that the variation of oxygen content affects the T_c 's of the 2212 and 2223 phases in opposite directions. The T_c of the 2223 phase decreased from 105 K to 89 K with weight loss. Morris *et al.* (109) found the T_c for the 2212 phase shifted reversibly over a range of at least 15 K by changing the oxygen concentration, and a much smaller shift of about 4 K occurred for the 2223 phase.

The oxygen loss means loss of the excess oxygen, which may reside mainly in the Bi-O layers or between the Bi-O layers, as reported by many groups (105, 110, 111). However, the exact positions of the excess oxygen atoms in the Bi-O plane have not been determined so far. Zhou *et al.* (111) have reported that the T_c of the oxide superconductor depends on both the density of oxygen vacancies in the CuO_2 planes and the content of interstitial oxygen in the Bi_2O_2 planes. They also proposed that the oxygen-vacancy ordering in the planes may be an essential factor that influences the superconductivity. Actually, the excess oxygen loss is the change in the kind of defects that were mentioned above, which is similar to the results reported by Bernard (112). So the viewpoint is that the change in the oxygen content changed the copper valency, accompanying the changes in the hole concentration in the conduction layers. Variation of the oxygen content changes the distribution of charge in the

copper oxide superconductor by a charge-transfer process. Such a process yields a striking correlation between the transition temperature T_c and the oxygen loss.

The TEM patterns in Figures 23-24 reveal sequences of satellites along the b-axes, which show that the structure is in fact modulated. As described in chapter II, the structural modulations are due to the numerous defects such as oxygen vacancies, metal site vacancies, interstitial oxygen, atomic displacement, stacking faults, metal atomic antisite, etc., and most defects form in or between the Bi-O layers. According to neutron diffraction data, Maeda (92) reported that even Cu atoms and oxygen atoms in the CuO_2 layer are displaced from their average positions due to the existence of the modulated structure in the Bi-O planes. So, in the Bi-Sr-Ca-Cu-O system, the existence of the complicated modulated structure has made the precise structural analysis almost impossible.

A 25.4 Å incommensurate superlattice, which was reported commonly by many research groups (43, 87, 90), appeared also in Figures 24-25. High-resolution electron microscope images show not only the 25.4 Å, but also a period of 27.0 Å, which was reported by Onozuka *et al.* (113). The other different modulation periods, rather than the uniform 25.4 Å superlattice, were reported by Hewat *et al.* (91) and Herrera *et al.* (89). In Figure 26, the extra reflections with periods of 38.7 Å and 72.6 Å appeared before the BC treatment. This

is probably due to the distribution of structural defects. The interesting result is that the extra satellite corresponding to the 72.6 Å periodicity disappeared after exposure of sample in the ballistic compressor. Without the high resolution electron microscope technique which can distinguish the individual atom columns, determining the type of change on the atomic scale could be very difficult. According to the fact that dimensions of the unit cell of the sample were not affected by the BC treatment, possible change in the structure can be inferred. A superstructure model based on the observations in electron diffraction patterns with superlattice reflections is proposed by Onozuka *et al.* (113), who attempt to explain the presence of 24.3 Å and 27 Å superstructure along the b-direction. The proposed superstructure is shown schematically in Figure 28 (113). The superstructure model is assumed to have the unit cell dimensions of a , Lb (L corresponds to the different modulation periods; for example, L is equal to 4.5 and 5.0 correspond to 24.3 Å and 27 Å, respectively), and c . The regions I and II correspond to the modulation periods of 24.3 Å ($L=4.5$) and 27 Å ($L=5.0$) along [010] direction. The regions I and II are shown in Figure 28 (a) and (b), and oxygen atoms are omitted for clarity. Viewed down the c -axis in Figure 28 (a) and (b), these structures illustrate the possible displacements of the atomic positions that correspond to the two periods in region I and II, respectively. In Figure 28 (c) and (d), the

proposed structures corresponding to the (a) and (b) along [100] show that the distance between two Bi-O layers varies and the other metal atoms displace relatively. This simple model shows the possibility of occurrence of a superlattice, which is caused by the displacements of metal atoms, but it omits the oxygen atoms. Actually, the displacements of Bi atoms and other metal atoms are possibly associated with the additional oxygen atoms or oxygen vacancies. Although the model is too simple, and does not represent the true incommensurability of superstructure reflections, from this

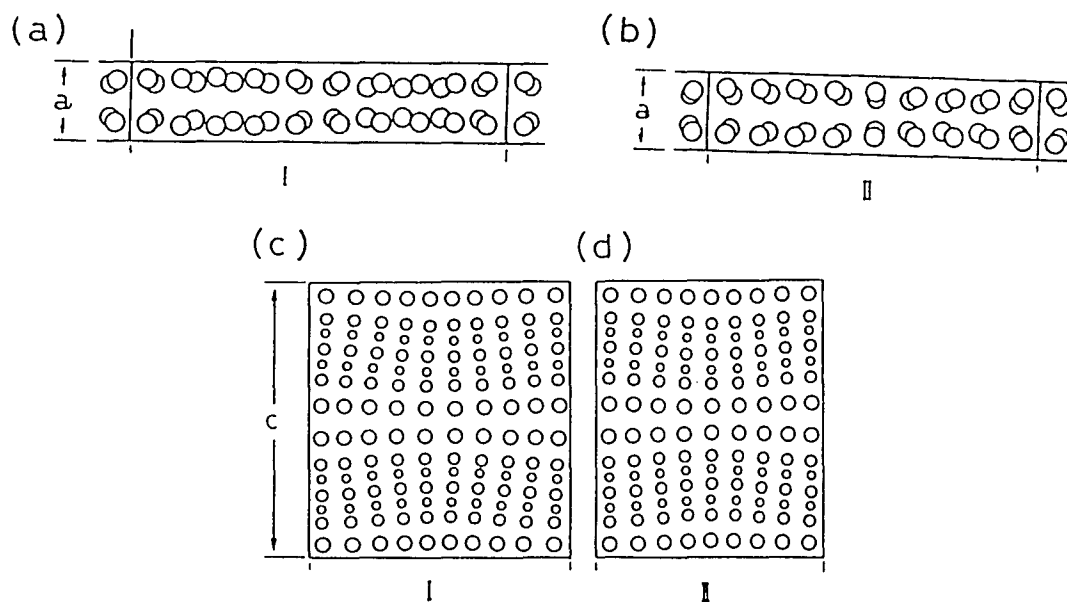


Figure 28. Schematic diagram of the proposed superstructure of Bi-based compounds. The unit cell of the superstructure model along [010], consisting of regions I and II. (a) and (b) Projections of Bi atoms along [001] in region I and II, respectively. (c) and (d) Projections of metal atoms along [100] in the region I and II, respectively. The large, medium and small circles represent Bi, Sr or Ca, and Cu atoms, respectively.

proposition of a superstructure model, the disappearance of the superlattice diffraction spots may be due to the distribution of defects in the sample as changed by the BC treatment. However it is difficult to determine exactly the changes which occurred.

Figures 26-27 show two types of twist boundary diffraction patterns, where successive layers rotate over an angle (91° and 81° , respectively) about the c-axis. These were found after exposure of samples in the ballistic compressor. This is possible because b-axes are approximately equal to a-axes for the unit cell.

The effect of a twist boundary on superconductivity is not yet clear. Yttrium compounds have a high density of twins. Varela et al. (114) suggested that the superconductivity enhancement in the twin boundaries region may be one of the reasons for the high T_c of the Y-compounds. Bobrov et al. (115) reported that the presence of the twin boundaries is probably the cause of the higher temperature superconduction in the yttrium system. For Bi-based compounds, the twist boundaries are not so frequently observed, so Hewat et al. (91) thought that the difference of twinning behavior in the Bi compounds and Y-compounds implies that twinning does not play an essential role in high T_c superconductivity. Han et al. (116) have taken electrical and magnetic measurements for a single twin boundary, but the preliminary results did not show significantly the effect of a single twin on the

superconducting properties. Our preliminary experimental results are not conclusive enough to demonstrate the effect of twist boundaries on superconductivity, but the enhancement of superconducting properties along with an increase of density of twist boundaries after exposure of samples in the ballistic compressor may have significance. It is likely that the detailed description of the complex structures of the Bi-based compounds will require single crystals and high-resolution imaging of the lattice by TEM.

SUMMARY

On the basis of available experimental data and the present observations, we summarize and discuss the system as follows. The ballistic compressor treatment offers a rapid heating and cooling process. The factor of pressure in this process is not very important because the pressures were not high enough to affect the superconducting properties of the exposed samples because of the high pressure coefficient (+2.0 K/GPa). This shows that the T_c increases 2 K under pressure of 1 GPa, as reported by Yoneda *et al.* (117). The resistance and susceptibility measurements performed have revealed the increase of T_c after the rapid heating and cooling. On the basis of SEM and EDS observations it is concluded that the surface of samples melted and the oxygen content decreased in the ballistic compressor treatment process. XRD investigations also indicated that the 2212 and

2223 phases increased and the 2201 phase decreased in proportion. TEM revealed effects on the modulation structure of Bi compounds which may be due to the change in the structural defects.

From the microscopic point of view, the explanation for the formation of the high T_c phase is an intergrowth process during rapid heating in the BC treatment. Due to the structural similarities of three phases of Bi-based compounds, intergrowths may exist in the real crystals. That is, individual crystals may be composed of layer units of two or more types. In Figure 2, the phases formed in the solid region of the Bi-Sr-Ca-Cu-O system suggest that the intergrowth phenomenon and phase-transformation process would occur at different firing temperature in air. The 2201, 2212, and other solid phases form below 800 °C. Above 800 °C, the 2212 and 2223 phase are stable.

Padam *et al.* (118) proposed that the intergrowth process is such that interfaces between the 2212 phase and Ca_2CuO_3 are created in a typical layered eutectic microstructure. Because of the large calcium and copper concentration differences between these two phases, calcium and copper atoms diffuse into the 2212 phase in a certain heat treatment. Therefore, the 2223 phase may nucleate and grow on the 2212 phase by adding one more Cu-O and Ca-O planes to the 2212 phase unit cell.

Oxygen is a very volatile element. In the ballistic

compressor treatment process, oxygen loss occurred. It has been suggested that the excess oxygen locates mainly in or between the double Bi-O layers, and the Bi-O layers are the electron transfer reservoirs. Therefore, the extra oxygen loss caused a variation of oxidation state of copper between Cu^{II} and Cu^{III} . It can be thought that the amount of electron transfer from the Cu-O layers to Bi layers increases, and hence the hole carrier density in the conduction layers increases too. It leads to the T_c increases through the hole concentration of the Cu-O plane. The rapid heating and quenching prevents significant oxygen pickup from the surrounding of samples because of insufficient time for oxygen to diffuse into the sample; in other words, this process freezes the structural defects in the copper oxide superconductors. This may explain the observations of increase in T_c by rapid quenching from high temperature.

There exists sufficient evidence that in copper-based oxides, superconductivity is primarily due to the charge carrier concentration in Cu-O layers. Usually, the hole concentration has been varied by the variation of the oxygen content in Bi compounds. It is well established that in the Bi system, the oxygen loss converts the cation Cu^{2+} to Cu^{3+} ions, which represent the real charge state on Cu. Actually, the real charge representation for the oxidation state is rounded off partly because they are never accurately known (54). The higher state of oxidation of copper increases the

number of holes in the Cu-O layers improving thereby the superconducting behavior. Bansal *et al.* (119) proposed that in the case of Bi-Sr-Ca-Cu-O compounds, calcium and strontium exist only in the 2+ charge state, in which electrons in Ca^{+2} and Sr^{+2} are strongly bound because their outermost electrons are in a closed shell. On the other hand, bismuth can exist in 1+, 3+ and 5+ charge states because its outermost electron shell is not closed. The copper ions get oxidized indirectly through bismuth ions. It may be thought that, due to the oxygen lost in the rapid heating and cooling process, the Bi^{3+} ions are reduced to Bi^{1+} ions according to the process $\text{Bi}^{3+} + \text{Cu}^{2+} + \text{O}^{1-} \rightarrow \text{Bi}^{1+} + \text{Cu}^{3+} + \text{O}$. And as the oxidation of copper increases, the hole concentration in the Cu-O layers increases too. Therefore, the oxygen is released from the sample and electrons transfer to a Bi-O layer from a Cu-O layer, thereby improving the superconducting behavior of this oxide cuprate superconductor.

CHAPTER V

CONCLUSIONS

Thin film samples and pellet superconductor samples with nominal composition of $\text{Bi}_2\text{Sr}_2\text{Ca}_{n-1}\text{Cu}_n\text{O}_{4+2n}$ were investigated before and after exposure in the ballistic compressor.

Resistance measurements of bulk and thin samples showed that the T_c can be increased by 3 - 6 K after BC treatment. A two-step shape of the resistance versus temperature curve was often observed, indicating that the formation of a high T_c phase occurred. Similar phenomena were observed in the diamagnetic behavior for the bulk and thin film samples. X-ray diffraction data showed increases of high T_c phases. This indicates that phase transformation occurred during the rapid heating, and the new phases were frozen in cooling during the process.

For the Bi-based compounds, the electron diffraction patterns showed strong modulation superstructure along the b-direction, and also showed extra superlattice of 38.7 Å and 72.6 Å. Both x-ray and electron diffraction patterns showed that the relative intensities of reflections were changed by the BC treatment. Worth noting is that the extra superlattice of 72.6 Å disappeared after exposure in the ballistic compressor, indicating possible change in the structural

defects of the cuprate superconductor.

SEM investigation of these samples showed that the BC treatment was limited to a depth of about 10 μm on the surface, and that a portion of the surface melted during exposure to hot and dense gas in the ballistic compressor. It was shown by EDS analysis that samples have inhomogeneous chemical compositions, and that oxygen loss occurred in the BC process.

It is thought that the oxygen loss catalyzed charge transfer from the charge transfer to the charge transfer reservoir from the CuO_2 planes and increased the hole concentration in the CuO_2 layers. This improved the superconducting behavior of this oxide cuprate compound.

REFERENCES

1. J. G. Bednorz and K. A. Müller, Z. Phys. B **64**, 189 (1986).
2. C. W. Chu, A lecture presented at the Superconducting Digital Circuits and Systems Conference, (1991).
3. H. Kamerlingh Onnes, Comm. Leiden, 120b (1911).
4. H. Kamerlingh Onnes, Comm. Leiden, 133a (1913).
5. H. Kamerlingh Onnes, Comm. Leiden, 139f (1914).
6. W. Meissner and R. Ochsenfeld, Naturwissenschaften **21**, 787 (1933).
7. W. H. Keesom and J. N. van den Ende. Comm. Leiden, 219b (1932).
8. W. L. Johnson. J. Appl. Phys. **50**, 1557 (1979).
9. J. M. Rowell, R. C. Dynes, and P. H. Schmidt, Academic Press, New York, (1980).
10. D. Jérôme, A. Mazaud, M. Ribault and K. Bechgaard, J. Phys. Lett. Paris, **41**, L-95 (1980).
11. H. Urayama, H. Yamochi, G. Saito, K. Nozawa, M. Kinishita, S. Sato, K. Oshima, A. Kawamoto and J. Tanaka, Chem. Lett. **55**, (1988).
12. Z. Fisk, D. W. Hess, C. J. Pethick, D. Pines, J. L. Smith, J. D. Thompson and J. O. Willis, Science **239**, 33 (1989).
13. J. K. Hylm, C. K. Jones, R. Mazelsky, R. A. Hein, J. W. Gibson, In Proceedings of the 9th International Conference on Low Temperature Physics, 600 (1965).
14. C. W. Chu and M. K. Wu, Phys. Rev. Lett. **58**, 405 (1987).
15. C. W. Chu and M. K. Wu, Phys. Rev. Lett. **58**, 908 (1987).
16. H. Maeda, Y. Tanaka, M. Fukutomi and T. Asano, Jpn. J. Appl. Phys. Lett. **27**, 2 (1988).

17. Z. Z. Sheng and A. M. Hermann, Nature **332**, 55 (1988).
18. T. R. Dinger, et al, Phys. Rev. Lett. **58**, 2687 (1987).
19. J. G. Bednorz and K. A. Müller, "Earlier and Recent Aspects of Superconductivity," Springer Series in Solid-State Sciences **90**, 45 (1990).
20. C. Cough M. Coldough, E. Fargan, R. Jordan, M. Deene, C. Muirhead, A. Rae, N. Thomas, J. Abell, and S. Sutton, Nature **326**, 855 (1987).
21. J. Imer, F. Patthey, B. Dardel, W. Sheneider, Y. Baer, Y. Baer, Y. Petroff, and A. Zettl, Phys. Rev. Lett. **62**, 336 (1989).
22. J. Torrance, Y. Tokura, A. Nazzal, A. Bezing, T. Huang, and S. Pavkin, Phys. Rev. Lett. **61**, 1127 (1988).
23. Vladimir Z. Kresin and Stuart A. Wolf, "Fundamentals of Superconductivity," Plenum Press, New York and London, 189 (1990).
24. A. Junod, Physica C **153-155**, 1078 (1988).
25. Y. Jean, J. Kyle, H. Nakanishi, P. Turchi, R. Howell, M. Fluss, A. Wachs, R. Meng, P. Hor, J. Huang, and C. Chu, Phys. Rev. Lett. **60**, 1069 (1988).
26. C. J. Gorter and H. G. B. Casimir, Physica **1**, 305 (1934).
27. F. London and H. London, Proc. Roy. Soc. (London) **A 149**, 71 (1935).
28. V. Ginzburg and L. Landau, Zh. Eksp. Teor. Fiz. **20**, 1064 (1950).
29. E. Maxwell, Phys. Rev. **78**, 477 (1950).
30. C. A. Reynolds, B. Serin, W. H. Wright, and L. B. Nesbitt, Phys. Rev. **78**, 487 (1950).
31. L. N. Cooper, Phys. Rev. **104**, 1189 (1956).
32. J. L. Bardeen, L. N. Cooper, and J. R. Schrieffer, Phys. Rev. **108**, 1175 (1957).
33. J. W. Lynn, "High Temperature Superconductivity", Springer-Verlag, New York, Berlin, Heidelberg, London, Paris, Tokyo, Hong Kong, 12 (1990).

34. D. Jerome, A. Hazaud, M. Ribault, and K. Bechgaard, J. Phys. Lett. **41**, L195 (1980).
35. G. Eliashberg, Sov. Phys.—JETP **13**, 1000 (1961).
36. R. W. G. Wyckoff, "Crystal Structures", Interscience, New York, 359 (1960).
37. I. K. Schuller, J. D. Jorgensen, Mater. Res. Coc. Bull., **27** (1989).
38. J. C. Phillips, "Physics of High- T_c Superconductors", Academic Press, Inc. 155 (1989).
39. A. W. Sleight, Physics Today **44**, 24 (1991).
40. N. Ichinose, (Waseda University, Tokyo), Personal Communication, (1992).
41. J. W. Lynn, "High Temperature Superconductivity", Springer-Verlag, New York, Berlin, Heidelberg, London, Paris, Tokyo, Hong Kong, 84 (1990).
42. J. M. Tarascon, W. R. McKinnon, Y. Lepage, N. Stoffel, and M. Giroud, Phys. Rev. B **38**, 8885 (1988).
43. J. L. Tallon, R. G. Buckley, P. W. Gilberd, M. R. Presland, I. w. M. Brown, M. E. Bowden, L. A. Christian, and R. Goguel, Nature **333**, 153 (1988).
44. B. Jayaram, P. C. Lanchester, M. T. Weller, J. R. Grasmeder, P. A. J. de Groot, and G. P. Rapson, J. Phys. Condens. Matter **1**, 477 (1989).
45. Y Matsui, S Takekawa, H. Nozaki, A. Umezono, E. Takayama Muromachi, and S. Horiuchi, Jpn. J. Appl. Phys. **27**, 1241 (1988).
46. V. Z. Kresin and S. A. Wolf, "Fundamentals of Superconductivity", Plenum Press. New York nad London, 209 (1991).
47. H. Rietschel and L. J. Sham, Phys. Rev. B **28**, 5100 (1983).
48. M. B. Maple, J. W. Chen, Y. Dalichaouch, T. Kohara, C. Rossel, M. Torikachvili, M. W. Elfresh, and J. D. Thompson, Phys. Rev. Lett. **56**, 2727 (1986).
49. J. R. Schrieffer, X. G. Wen, and S. C. Zhang, Phys. Rev. Lett. **60**, 944 (1988).

50. J. C. Phillips, "Physics of High- T_c Superconductors", Academic Press, Inc., 306 (1989).
51. V. Z. Kresin and S. A. Wolf, "Fundamentals of Superconductivity", Plenum Press, New York and London, 22 (1990).
52. J. D. Jorgensen, Physics Today **44**, 34 (1991).
53. J. G. Bednorz and K. A. Müller, "Earlier and Recent Aspects of Superconductivity". Springer-Verlag, 50 (1990).
54. A. W. Sleight, Science **242**, 1519 (1988).
55. J. M. Wheatley, T. C. Hsu, and P. W. Anderson, Phys. Rev. B **37**, 5897 (1988).
56. A. W. Sleight, W. E. Hatfield, and J. H. Miller, "High-Temperature Superconducting Materials", Dekker, New York, 1-36 (1988).
57. J. C. Fuggle, Phys. Rev. B **37**, 123 (1988).
58. R. Kossovsky, B. Raveau, D. Wohlleben, and S. K. Patapis, "Physics and Materials Science of High Temperature Superconductors, II", Kluwer Academic Publishers, 119 (1992).
59. R. J. Cava, A. W. Hewat, E. A. Hewat, B. Batlogg, M. Marezio, K. M. Rabe, J. J. Krajewski, W. F. Peck Jr, L. W. Rupp Jr, Physica C **165**, 419 (1990).
60. J. D. Jorgensen, P. Lightfoot, S. Pei, Supercond. Sci. Technol. **4**, S11 (1991).
61. J. D. Jorgensen, B. Dabrowski, S. Pei, D. R. Richards, D. G. Hinks, Phys. Rev. B **40**, 2187 (1989).
62. R. J. Cava, B. Batlogg, R. B. van Dover, J. J. Krajewski, J. V. Waszczak, R. M. Flemming, W. F. Peck Jr, L. W. Rupp Jr, P. Marsh, A. C. W. P. James, L. F. Schneemeyer, Nature **345**, 602 (1990).
63. M. Nagoshi, T. Suzuki, Y. Fukuda, K. Terashima, Y. Nakanishi, M. Ogita, A. Tokiwa, Y. Syono. and M. Tachiki, Phys. Rev. B **43**, 10445 (1991).
64. B. W. Veal, H. You, A. P. Paulikas, H. Shi, U. Fan, and J. W. Downey, Phys. Rev. B **42**, 4770 (1990).

65. R. J. Cave, A. W. Hewat, E. A. Hewat, B. Batlogg, M. Marezio, K. M. Rabe, J. J. Krajeuski, W. F. Peck Jr., and L. W. Rupp Jr., Physica C **165**, 419 (1990).
66. J. D. Jorgensen, S. Pei, P. Lightfoot, A. P. Paulikas, B. W. Veal, Physica C **167**, 571 (1990).
67. J. L. Tallon, R. G. Buckley, P. W. Gilberd, M. R. Presland, I. W. M. Brown, M. E. Bowden, L. A. Christian, and R. Goguel, Nature **333**, 153 (1988).
68. M. Takano, Nature **333**, 200 (1988).
69. G. Bucher, J. Karpinski, E. Kaldis and P. Wachter, Physica C **167**, 478 (1989).
70. B. Okai and M. Kosuge, K. Takahashi, and M. Ohta, Jpn. J. Appl. Phys. **27**, 674 (1988).
71. K. Kumagai and M. Kuisu, Jpn. J. Appl. Phys. **27**, 1029 (1988).
72. S. Tamura, S. Takekawa, H. Nozaki, and A. Umezono, J. Phys. Soc. Jpn. **57**, 2215 (1989).
73. R. J. Wijngaarden, H. K. Hemmes, E. N. van Eenige, R. Griessen, A. A. Menovsky, and M. J. V. Menken, Physica C **158**, 237 (1989).
74. C. W. Chu, P. H. Hor, J. G. Lin, Q. Xiong, Z. J. Huang, R. L. Meng, Y. Y. Xue, and Y. C. Jean, Physica C **165**, (1991).
75. R. Y. Jin, F. Shi, W. Z. Ran, Z. H. Shi and S. Z. Zhou, Physica C **158**, 225 (1989).
76. C. J. Kim, C. K. Rhee, H. G. Lee, C. T. Lee, S. J-L. Kang, and D. Y. Won, Jpn. J. Appl. Phys. **28**, 45 (1989).
77. G. C. Tu, F. H. Chen, and H. S. Koo, Supercond. Sci. Technol. **3**, 134 (1990).
78. M. Pissas, D. Niarchos, C. Christides, and M. Anagnostou, Supercond. Sci. Technol. **3**, 128 (1990).
79. I. Takekazu, M. Hiromasa, and S. Takashi, Jpn. J. Appl. Phys. **27**, 1626 (1988).
80. M. Yoshimura, T. H. Sung, N. Ishizawa, and Z. Nakagawa, Jpn. J. Appl. Phys. **28**, 424 (1989).

81. S. L. Furcone and Y. M. Chiang, Appl. Phys. Lett. **52**, 2180 (1988).
82. J. W. Ekin, A. J. Panson, and B. A. Blankenship, Appl. Phys. Lett. **52**, 331 (1988).
83. Paula Posar, "Magnetic Susceptibility", Superconductor, **2**, 28 (1989).
84. M. Takeo, Q. A. Holmes, and A. Y. Chen, J. Appl. Phys. **38**, 3544 (1967).
85. J. Dash, M. Takeo, A. R. Trzynka, J. M. Roush, A. M. Kasaaian, F. B. Brace, H. Takeo, and P. G. Weaver, Marcel Dekker, "Metallurgical Applications of Shock-Wave and High-Strain-Rate Phenomena", Marcel Dekker, 1051 (1986).
86. A. Straub, Thesis, (July 10, 1992). (Portland State University)
87. Q. Duan and J. Dash, Proceedings of the 12th International Congress for Electron Microscopy, San Francisco 4, 90 (1990).
88. Q. Duan, J. Dash, M. Takeo, and J. Huang, J. Appl. Phys. **69**, 4897 (1991).
89. R Herrera, A Gómez, P Schabes-Retchkiman, and M José-Yacamán, Supercond. Sci. Technol., **3**, 84 (1990).
90. J. M. Tarascon, Y. LePage, L. H. Greene, B. G. Bagley, P. Barboux, D. M. Hwang, G. W. Hull, W. R. McKinnon, and M. Giroud, Phys. Rev. B **38**, 2504 (1988).
91. E. A. Hewat, M. Dupuy, P. Bordet, J. J. Capponi, C. Chailout, J. L. Hodeau, and M. Marezio, Nature, **333**, 53 (1988).
92. A. Maeda, M. Hase, I. Tsukada, K. Noda, S. Takebayashi, and K. Uchinokura, Phys. Rev. B **41**, 6418 (1990).
93. H. Takagi, H. Eisaki, S. Uchida, A. Maeda, S. Tajima, K. Uchinokura, and S. Tanaka, Nature **332**, 236 (1988).
94. H. W. Zandbergen, U. K. Huang, M. J. V. Menken, J. N. Li, K. Kadowaki, A. A. Menovsky, G. van Tendeloo, and S. Amelinck, Nature **332**, 620 (1988).
95. X. Jhu, S. Feng, J. Zhang, G. Lu, K. Chen, K. Wu, and Z. Gan, Mod. Phys. Letts. B **3**, 707 (1989).

96. S. Bartram, "Handbook of X-Rays", (ed. E. Kaelble) McGraw-Hill Book Company, New York, San Francisco, Toronto, London, Sydney, 17-1 (1967).
97. L. Ganapathi, J. Narayan, and A. Kumar, Appl. Phys. Lett. **55**, 1460 (1989).
98. J. Polonka, Ming Xu, Qiang Li, A. I. Goldman, and D. K. Finnemore, Appl. Phys. Lett. **59**, 3640 (1991).
99. S. Lösch, H. Budin, Ko. Eibl, M. Hartmann, T. Rentschler, M. Rygula, S. Kemmler-Sack, and R. P. Huebener, Physica C **177**, 271 (1991).
100. M. F. C. Ladd and R. A. Palmer, "Structure Determination by X-Ray Crystallography", Plenum Press. New York and London, 155 (1977).
101. H. P. Klug, and L. E. Alexander, "X-ray Diffraction Procedures", John Wiley & Sons, New York, London. Sydney, Toronto, 618 (1974).
102. P. Scherrer, Göttinger Nachrichten, **2**, 98 (1918).
103. Y. Kohta, Y. Masamichi, and N. Motoo, Jpn. J. Appl. Phys. **27**, 12324 (1988).
104. A. Kikuchi, M. Matsuda, M. Takata, M. Ishii, T. Yamashita, and H. Koinuma, Jpn. J. Appl. Phys. **27**, 2300 (1988).
105. D. Shi, M. Tang, K. Vandervoort, and H. Claus, Phys. Rev. B **39**, 9091 (1989).
106. J. Zhao and M. S. Seehra, Physica C **159**, 639 (1989).
107. J. Zhao, M. Wu, W. Abdul-Razzaq, and M. S. Seehra, Physica C **165**, 135 (1990).
108. S. E. Morris, C. T. Hyltgren, A. M. Markelz, J. Y. T. Wei, N. G. Asmar, and J. H. Nickel, Phys. Rev. B **39**, 6612 (1989).
109. I. M. Tang, K. Eaiprasertsak, R. Chitaree, and P. Winotai, Physica C **167**, 491 (1990).
110. C. J. Zhou, D. L. Tao, and T. G. Chen, Physica C **180**, 365 (1991).
111. R. Bernard, Physics Today **45**, 53 (1992).

112. T. Onozuka, T. Kajitani, M. Hirabayashi, H. Sato, and T. E. Mitchell, Jpn. J. Appl. Phys. **28**, 1775 (1989).
113. C. Varea and A. Robledo, "Oxygen Ordering and Interfacial Superconductivity at Twin Boundaries in A Landau-Ginzburg Superconductor Oxide Model", Plenum Press, New York, 1033 (1987).
114. V. S. Bovrov and M. A. Lebyodkin, Physica C **178**, 411 (1991).
115. P. D. Han, A. Asthana, Z. Xu, L. Chang, and D. A. Payne, Phys. Rev. B **43**, 5437 (1991).
116. T. Yoneda, Y. Mori, Y. Akahama, M. Kobayashi, and H. Kawamura, Jpn. J. Appl. Phys. **29**, 1396 (1990).
117. G. K. Padam, R. B. Tripathi, M. Sharma, D. K. Suri, S. U. M. Rao, K. C. Nagpal, and B. K. Das, Solid State Comm. **80**, 271 (1991).
118. T. K. Bansal, B. Sadhana, and R. G. Mendiratta, Solid State Commu. **76**, 1027 (1991).